CFD Simulation of Vortex Induced Vibration of a Cylindrical Structure

Muhammad Tedy Asyikin

NORWEGIAN UNIVERSITY OF SCIENCE AND TECHNOLOGY
DEPARTMENT OF CIVIL AND TRANSPORT ENGINEERING

Report Title:	Date: June 11, 2012.
CFD Simulation of Vortex Induced Vibration of a Cylindrical Structure	No. of pages (incl. appendices): 83
	Master Thesis X Project Work

Name:
    Muhammad Tedy Asyikin

Professor in charge/supervisor:
    Hans Bihs

Other external professional contacts/supervisors:
    -

Abstract:

This thesis presents the investigation of the flow characteristic and vortex induced vibration (VIV) of a cylindrical structure due to the incompressible laminar and turbulent flow at Reynolds number 40, 100, 200 and 1000. The simulations were performed by solving the steady and transient (unsteady) 2D Navier-Stokes equation. For Reynolds number 40, the simulations were set as a steady and laminar flow and the SIMPLE and QUICK were used as the pressure-velocity coupling scheme and momentum spatial discretization respectively. Moreover, the transient turbulent flow was set for Re 100, 200 and 1000 and SIMPLE and LES (large Eddy Simulation) were selected as the pressure-velocity coupling solution and the turbulent model respectively.

The drag and lift coefficient (Cd and Cl) were obtained and verified to the previous studies and showed a good agreement. Whilst the vibration frequency (fvib), the vortex shedding frequency (fv), the Strouhal number (St) and the amplitude of the vibration (A) were also measured.

Keywords:

1. CFD Simulation
2. VIV
3. Cylinder

Muhammad Tedy Asyikin
(signature)

NTNU
Norwegian University of Science
and Technology

Faculty of Engineering Science
and Technology
Department of Civil and
Transport Engineering

Division: Marine Civil
Engineering
Postal address:
Høgskoleringen 7A
7491 Trondheim
Phone: 73 59 46 40
Telefax: 73 59 70 21

Master Thesis

Spring 2012

Student: **Muhammad Tedy Asyikin**

CFD Simulation of Vortex Induced Vibration
of a Cylindrical Structure

Background:

This thesis presents the investigation of the flow characteristic and vortex induced vibration (VIV) of a cylindrical structure due to the incompressible laminar and turbulent flow at Reynolds number 40, 100, 200 and 1000. The simulations are performed by solving the steady and transient (unsteady) 2D Navier-Stokes equation. For Reynolds number 40, the simulations were set as a steady and laminar flow and the SIMPLE and QUICK were used as the pressure-velocity coupling scheme and momentum spatial discretization respectively. Moreover, the transient turbulent flow was set for Re 100, 200 and 1000 and SIMPLE and LES (large Eddy Simulation) were selected as the pressure-velocity coupling solution and the turbulent model respectively.

The drag and lift coefficient (Cd and Cl) were obtained and verified to the previous studies and showed a good agreement. Whilst the vibration frequency (f_{vib}), the vortex shedding frequency (f_v), the Strouhal number (St) and the amplitude of the vibration (A) were also measured.

Objective of the thesis work

The main objectives of this thesis are:
1. To investigate the flow pattern and characteristic around a cylindrical structure.
2. To investigate the vibrations of a cylindrical structure.

Scope of work (work plan)

The thesis work includes, but is not limited to, the following:
1. Familiarization with the concept of flow around cylindrical structure.
2. Understanding the vibration phenomena of cylindrical structure.
3. Determining the important features of the problem of flow around cylindrical structure.
4. Performing the simulation of CFD
   a. Defining the simulation goals.
   b. Creating the model geometry and mesh.
   c. Setting up the solver and physical model.
   d. Computing and monitoring the solution.
   e. Examining and saving the result.
   f. Consider revisions to the numerical or physical model parameters, if necessary.
5. Compare and discuss any findings and results.

General about content, work and presentation

The text for the master thesis is meant as a framework for the work of the candidate. Adjustments might be done as the work progresses. Tentative changes must be done in cooperation and agreement with the professor in charge at the Department.

In the evaluation thoroughness in the work will be emphasized, as will be documentation of independence in assessments and conclusions. Furthermore the presentation (report) should be well organized and edited; providing clear, precise and orderly descriptions without being unnecessary voluminous.

Submission procedure

On submission of the thesis the candidate shall submit a CD with the paper in digital form in pdf and Word version, the underlying material (such as data collection) in digital form (eg. Excel). Students must submit the submission form (from DAIM) where both the Ark-Bibl in SBI and Public Services (Building Safety) of SB II has signed the form. The submission form including the appropriate signatures must be signed by the department office before the form is delivered Faculty Office.

Documentation collected during the work, with support from the Department, shall be handed in to the Department together with the report.

According to the current laws and regulations at NTNU, the report is the property of NTNU. The report and associated results can only be used following approval from NTNU (and external cooperation partner if applicable). The Department has the right to make use of the results from the work as if conducted by a Department employee, as long as other arrangements are not agreed upon beforehand.

Start and submission deadlines

The work on the Master Thesis starts on January 16, 2012.
The thesis report as described above shall be submitted digitally in DAIM at the latest at 3pm June 11, 2012.

Professor in charge: **Hans Bihs**

Trondheim, June 11, 2012.

_____
                    Hans Bihs

ABSTRACT

This thesis presents the investigation of the flow characteristic and vortex induced vibration (VIV) of a cylindrical structure due to the incompressible laminar and turbulent flow at Reynolds number 40, 100, 200 and 1000. The simulations were performed by solving the steady and transient (unsteady) 2D Navier-Stokes equation. For Reynolds number 40, the simulations were set as a steady and laminar flow and the SIMPLE and QUICK were used as the pressure-velocity coupling scheme and momentum spatial discretization respectively. Moreover, the transient turbulent flow was set for Re 100, 200 and 1000 and SIMPLE and LES (large Eddy Simulation) were selected as the pressure-velocity coupling solution and the turbulent model respectively.

The drag and lift coefficient (Cd and Cl) were obtained and verified to the previous studies and showed a good agreement. Whilst the vibration frequency (f_{vib}), the vortex shedding frequency (f_v), the Strouhal number (St) and the amplitude of the vibration (A) were also measured.

Keywords :

1. CFD Simulation
2. VIV
3. Cylindrical Structure

ACKNOWLEDGEMENTS

TABLE OF CONTENTS

REFERENCES

APPENDIX A - Problem Description

APPENDIX B - UDF of 6DOF Solver

APPENDIX C - ANSYS Fluent Setup

LIST OF FIGURES

LIST OF TABLES

LIST OF SYMBOLS

Re	Reynolds number
D	cylinder diameter
U	the flow velocity
v	kinematic viscocity
St	Strouhal number
Fv, ω_s	vortex shedding frequency
F_L	the lift force
F_D	the drag force
$\hat{F}_L$	amplitudes of the oscillating lift
$\hat{F}_D$	amplitudes of the oscillating drag
$\bar{F}_D$	the mean drag
ϕ_s	the phase angle
$\hat{C}_L$	lift coefficient of the oscillating lift
$\hat{C}_D$	drag coefficient of the oscillating drag
$\bar{C}_D$	mean drag coefficient
ρ	fluid density
L	cylinder length
U_m	maximum flow velocity
T	period
A	displacement amplitude
$U_{red,true}$	true reduced velocity
$U_{red,nom}$	nominal reduced velocity
fn	natural frequency
KC	Keulegan-Karpenter number
Fr	Froude's number
g	gravity force
m	cylinder mass
c	damping factor
k	stiffness
ζ	the total damping factor

1 INTRODUCTION

1.1. Background

Vibration of a cylindrical structure, i.e. pipeline and riser, is an important issue in designing of offshore structure. Vibrations can lead to fatigue damage on the structure when it is exposed to the environmental loading, such as waves and currents. In recent years, the exploration of oil and gas resources has advanced into deep waters, thousands of meters below sea surface, using pipelines and risers to convey the hydrocarbon fluid and gas.

For deep water, there will only be current force acting on the structure. As wave forces reduce with depth, they become insignificant in very deep water. In this case, the interaction between the current and the structure can give rise to different forms of vibrations, generally known as flow-induced vibrations (FIV).

The availability of powerful super computers recently has given an opportunity to users in performing simulations in order to obtain optimum results as well as in numerical modeling of fluid dynamics. The numerical modeling in fluid dynamics, so-called computational fluid dynamics (CFD), therefore, becomes very important in the design process for many purposes as well as in marine industry.

By the need of offshore oil and gas production in deepwater fields, numerical simulation of offshore structure has been an active research area in recent years. Experiments are sometimes preferable to provide design data and verification. However, offshore structures have aspect ratios that are so large that model testing is constrained by many factors, such as experimental facility availability and capacity limits, model scale limit, difficulty of current profile generation, and cost and schedule concerns. Under such conditions, CFD simulation provides an attractive alternative to model tests and also provides a cost effective alternative.

1.2.   Scope of Work

The thesis work includes, but is not limited to, the following:
1.   Familiarization with the concept of flow around cylindrical structure.
2.   Understanding the vibration phenomena of cylindrical structure.
3.   Determining the important features of the problem of flow around cylindrical structure.
4.   Performing the simulation of CFD
       a.   Defining the simulation goals.
       b.   Creating the model geometry and mesh.
       c.   Setting up the solver and physical model.
       d.   Computing and monitoring the solution.
       e.   Examining and saving the result.
       f.   Consider revisions to the numerical or physical model parameters, if necessary.
5.   Compare and discuss any findings and results.

1.3.   Project Objectives

The main objectives of the thesis work are:
1.   To investigate the flow pattern characteristic around cylindrical structure.
2.   To investigate the vibrations of cylindrical structure due to the flow (current).

1.4.   Structure of the Report

The thesis is organized in five main chapters. Chapter 1 is an introduction. Chapter 2 consists of the theory and information regarding flow around cylindrical structure. Chapter 3 explains the CFD theories and the simulation of CFD. Chapter 4 gives the analysis and discussions from the result. Finally, Chapter 5 gives the conclusions and recommendations.

Chapter 1 is an introduction of the thesis work. It describes a general overview of the thesis work. The objectives and the structure of the report are also described in this chapter.

Chapter 2 is the explanation of the theories regarding the flow around cylindrical structure. This chapter also describes a similar experimental work that had been carried out, as a comparison to the simulation results later on.

Chapter 3 is an explanation of CFD. This section describes a theory in CFD as well as its simulation. The simulation of CFD consists of some procedures, which includes 1) defining the simulation goals, 2) creating the model geometry and mesh, 3) setting up the

solver and physical model, 4) computing and monitoring the solution, 5) examining and saving the result and 6) revisions, if necessary.

Chapter 4 is the result and discussion part. It presents the results of the CFD simulation from Chapter 3. It also includes the discussion of the results by comparing to those of similar previous experimental works. The last part of this chapter gives the summary of the results.

Finally, Chapter 5 is the conclusions and recommendations part. This chapter gives the conclusions from Chapter 4. The recommendations are given for any further work related to this thesis topic.

2 FLOW AROUND CYLINDRICAL STRUCTURE

2.1. Basic Concept

When a structure, in this case, a cylindrical structure subjected to the fluid flow, somehow the cylinder might experience excitations or vibrations. These vibrations known as the flow induced vibrations can lead to the fatigue damage to the structure. Hence, it is essential to take those vibrations into considerations whilst designing many structures, particularly the cylindrical structure.

2.1.1. Regime of Flow
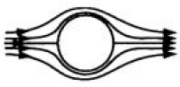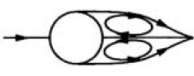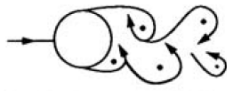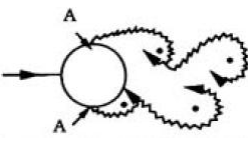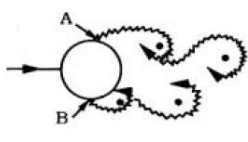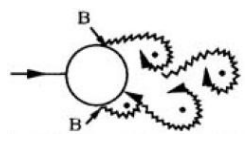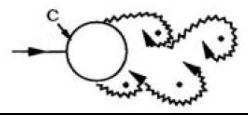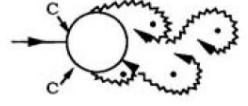
One of the non dimensionless hydrodynamic numbers that is used to describe the flow around a smooth circular cylinder is the Reynolds number (Re). By the definition, the Reynolds number is the ratio of the inertia forces to viscous forces and formulated as

$$Re = \frac{DU}{v} \qquad\qquad (2.1)$$

in which D is the diameter of the cylinder, U is the flow velocity and v is the kinematic viscosity of the fluid.

Flow regimes are obtained as the result of tremendous changes of the Reynolds number. The changes of the Reynolds number create separation flows in the wake region of the cylinder, which are called vortices. At low values of Re (Re < 5), there no separation occurs. When the Re is further increased, the separation starts to occur and becomes unstable and initiates the phenomenon called vortex shedding at certain frequency. As the result, the wake has an appearance of a vortex street as can be seen in Table 2.1.

Table 2.1.   Flow regime around smooth, circular cylinder in steady current, adapted from [14].

	No separation Creeping flow	Re < 5
	A fixed pair of symmetric vortices	5 < Re < 40
	Laminar vortex street	40 < Re < 200
	Transition to turbulence in the wake	200 < Re < 300
	Wake completely turbulent. A. Laminar boundary layer separation	$300 < Re < 3x10^5$ Subcritical
	A. Laminar boundary layer separation . B. Turbulent boundary layer separation, but boundary layer laminar	$3x10^5 < Re < 3.5 \text{ x } 10^5$ Critical (Lower transition)
	B. Turbulent boundary layer separation:the boundary layer part1y laminar partly turbulent	$3.5 \text{ x } 10^5 < Re < 1.5 \text{ x }$ 10^6 Supercritical
	C. Boundary layer completely turbulent at one side	$1.5 \text{ x } 10^6 < Re < 4 \text{ x}10^6$ Upper transition
	C. Boundary layer completely turbulent at two sides	$4 \text{ x } 10^6 < Re$ Transcritical

2.1.2. Vortex Shedding

The Vortex shedding phenomenon appears when pairs of stable vortices are exposed to small disturbances and become unstable at Re greater than 40. For these values of Re, the boundary layer over the cylinder surface will separate due to the adverse pressure gradient imposed by the divergent geometry of the flow environment at the rear side of the cylinder.

As mentioned in the previous section, vortex shedding occurs at a certain frequency, which is called as vortex shedding frequency (f_v). This frequency normalized with the flow velocity U and the cylinder diameter D, can basically be seen as a function of the Reynolds number. Furthermore, the normalized vortex-shedding frequency is called Strouhal number (St), and formulated as:

$$St = \frac{f_v D}{U} \qquad\qquad (2.2)$$

The relationship between Re and St can be shown in Figure 2.1.
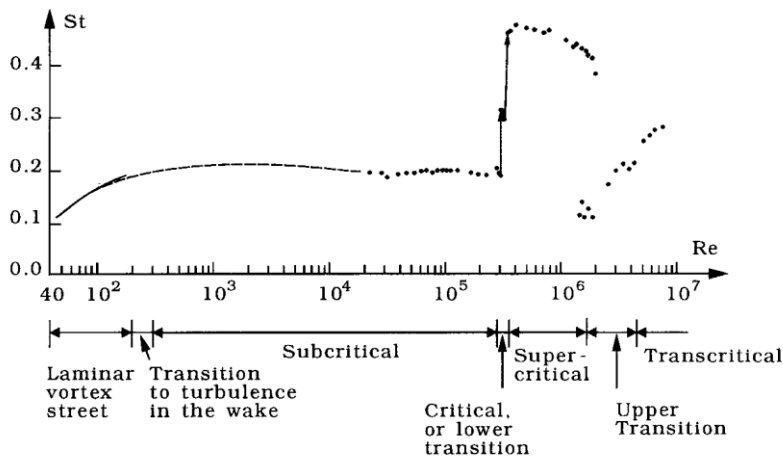
Fig. 2.1. Strouhal number for smooth circular cylinder, adapted from Sumer [14].

The large increase in St at the supercritical region is caused by the delay of the boundary separation. It is known that the separation point of the subcritical regime is different from that of the supercritical regime as shown in Figure 2.2. At the supercritical flow regime, the boundary layers on both sides of the cylinder are turbulent at the separation point. Consequently, the boundary layer separation is delayed since the separation point moves downstream. At this point, the vortices are close to each other and create faster rate than the rate in the subcritical regime, thereby leading to higher values of the Strouhal number.
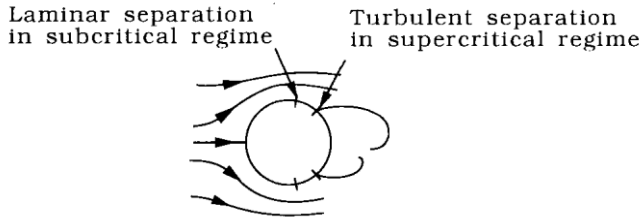
Fig. 2.2. Separation point of the subcritical regime and supercritical regime, adapted
Sumer [14].

When Re reaches the value of 1.5 x 10^6, the boundary layer completely becomes
turbulent at one side and laminar at the other side. This asymmetric situation is called the
lee-wake vortices. What happens next is that lee-wake vortices inhibit the interaction of
these vortices, resulting in an irregular and disorderly vortex shedding. When Re is
increased to values larger than 4.5 x 10^6 (transcritical regime), the regular vortex
shedding is re-established and St takes the values of 0.25 – 0.30.

2.1.3. Drag and Lift Forces

As the result of the periodic change of the vortex shedding, the pressure distribution of
the cylinder due to the flow will also change periodically, thereby generating a periodic
variation in the force components on the cylinder. The force components can be divided
into cross-flow and in-line directions. The force of the cross-flow direction is commonly
named as the lift force (F_L) while the latter is named as the drag force (F_D). The lift force
appears when the vortex shedding starts to occur and it fluctuates at the vortex shedding
frequency. Similarly, the drag force also has the oscillating part due to the vortex
shedding, but in addition it also has a force as a result of friction and pressure difference;
this part is called the mean drag. Both of the lift and drag forces are formulated as
follows:

$$F_L = \hat{F}_L sin(\omega_s t + \phi_s) \tag{2.3}$$

$$F_D = \bar{F}_D + \hat{F}_D sin(2\omega_s t + \phi_s) \tag{2.4}$$

$\hat{F}_L$ and $\hat{F}_D$ are the amplitudes of the oscillating lift and drag respectively and $\bar{F}_D$ is the
mean drag. The vortex shedding frequency is represented by $\omega_s = {2\pi}/{f_v}$, and ϕ_s d is
the phase angles between the oscillating forces and the vortex shedding.

An experiment performed by Drescher in 1956 [5] which is described in Sumer [14]
traced the drag and lift forces from the measured pressure distribution as shown in
Figure 2.3. From the figure, it can be seen that the drag and lift forces oscillate as a
function of the vortex shedding frequency.
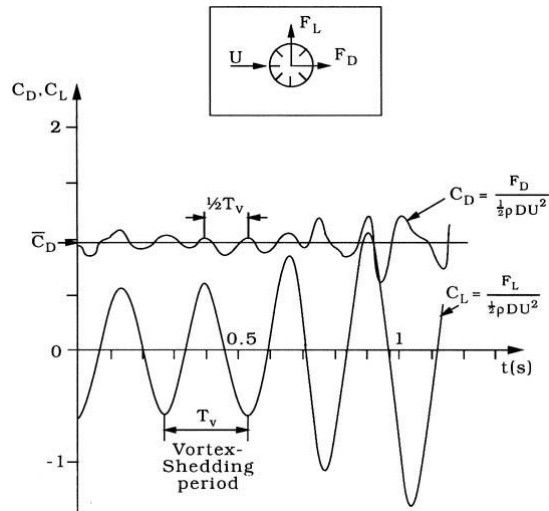
Fig. 2.3. Oscillating drag and lift forces traces, adapted from Sumer [14].

C_D and C_L are the dimensionless parameters for drag and lift forces respectively, and can be derived as:

$$\hat{C}_L = \frac{\hat{F}_L}{1/_2\rho L D U^2} \qquad\qquad (2.5)$$

$$\hat{C}_D = \frac{\hat{F}_D}{1/_2\rho L D U^2} \qquad\qquad (2.6)$$

$$\bar{C}_D = \frac{\bar{F}_D}{1/_2\rho L D U^2} \qquad\qquad (2.7)$$

where ρ, L, D and U are the fluid density, cylinder length, cylinder diameter and flow velocity respectively.

2.1.4. Other Hydrodynamic Numbers

Other hydrodynamic numbers, which are dimensionless parameters that are often used to study flow induced vibration, apart from Re and St that have been mentioned earlier, will be described briefly in the following sections.

Keulegan-Carpenter Number, *KC*

The Keulegan-Carpenter number is used to predict the flow separation around a body and whether the drag or inertia terms dominate in the Morison formula. It is also an important parameter to describe harmonic oscillating flows and is formulated as:

$$KC = \frac{U_m T}{D} = \frac{2\pi A}{D} \tag{2.8}$$

where U_m is the maximum velocity of the flow during one period T, D is the cylinder diameter and A is the displacement amplitude of the fluid.

Reduced Velocity, U_{red}

Reduced velocity can be divided into two types, true reduced velocity ($U_{red,true}$) and nominal reduced velocity ($U_{red,nom}$). The true reduced velocity is based on the frequency at which the cylinder is actually vibrating (f_n) whilst the nominal reduced velocity is based on the nominal natural frequency (f_{n0}), e.g. natural frequency in still water. Both are formulated as follows:

$$U_{red,true} = \frac{U}{f_n D} \tag{2.9}$$

$$U_{red,nom} = \frac{U}{f_{n0} D} \tag{2.10}$$

This number is a useful parameter to present the structure response along the lock-in range.

Froude Number, F_r

The Froude number is the key parameter in prediction of free surface effects, for instance the effect of waves on ships. This number is always used in model testing in waves and formulated as the following:

$$F_r = \frac{U}{(gL)^{0.5}} \tag{2.11}$$

where the g is the gravity force and L is the structure length.

Roughness

The surface roughness is of importance in many ways. It will influence the vortex shedding frequency. Increasing roughness will decrease Re at which transition to turbulence occurs. Roughness is often measured as the ratio of the average diameter of the roughness features, k, divided by the cylinder diameter D.

2.2. Vortex Induced Vibration

In this section, the theory of the vortex induced vibration will be described, particularly for cylindrical structure. It covers the solution to the vibration equation, structure and fluid damping, vibration of cylindrical structure and suppression of vibrations.

2.2.1. Solution to Vibration Equation

The sketch of the classic flow around cylindrical structure can be drawn as shown in Figure 2.4. A free vibration of an elastically mounted cylinder is represented by an idealized description of a vibrating structure.
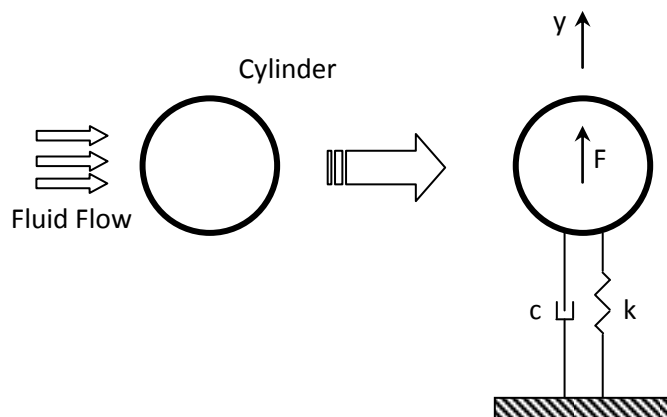
Fig. 2.4. Idealized description of a vibrating structure.

In this thesis, the structure is conditioned as a vibration-free elastically cylinder. It means that the cylinder is free to respond the vibrations. This condition is useful to find amplitude, frequency and phase angle of a vibrating cylinder and helpful in studying flow-visualization of the wake of the cylinder.

The differential motion equation of the system shown in Figure 2.4 is formulated as:

$$m\,\ddot{y}(t) + c\,\dot{y}(t) + k\,y(t) = F(t) \qquad (2.12)$$

in which m is the total mass of the system and dot over the symbols indicates differentiation with respect to time. For a free vibration system, i.e. no external forces working on the system (F=0), the solutions can, therefore, be differentiated into two conditions: without and with viscous damping.

Free vibrations without viscous damping

For free vibrations without viscous damping, the equation of motion will be

$$m\,\ddot{y}(t) + k\,y(t) = 0 \qquad\qquad (2.13)$$

Since *m* and *k* are positive, the solution is

$$y = A_y cos(\omega_v t) + B_y sin(\omega_v t) \qquad\qquad (2.14)$$

where A_y is the amplitude of vibrations and ω_v is the angular frequency of the motion, and formulated as

$$\omega_v = \sqrt{k/m} \qquad\qquad (2.15)$$

Free vibrations with viscous damping

In this case, the viscous damping in non-zero, therefore the equation of motion becomes:

$$m\,\ddot{y}(t) + c\,\dot{y}(t) + k\,y(t) = 0 \qquad\qquad (2.16)$$

The solution of Eq. (2.16) could be in an exponential form:

$$y = C e^{rt} \qquad\qquad (2.17)$$

By inserting Eq. (2.17) into Eq. (2.16), an auxiliary equation will be obtained as follows:

$$mr^2 + cr + k = 0 \qquad\qquad (2.18)$$

The two r values are calculated by

$$\left.\begin{matrix} r_1 \\ r_2 \end{matrix}\right\} = \frac{1}{2m}\left[-c \pm \sqrt{c^2 - 4mk}\right] \qquad\qquad (2.19)$$

As the result, the general solution of this case is

$$y = C_1 e^{r_1 t} + C_2 e^{r_2 t} \qquad\qquad (2.20)$$

The solution of Eq. (2.20) depends on the square root of (c^2 - 4*mk*), i.e. c^2 > 4*mk* (case 1) and c^2 < 4*mk* (case 2).

For case 1, the values of r_1 and r_2 are real. Therefore, C_1 and C_2 must be determined from the initial conditions, for example, for $t = 0, y = A_y$ and $\dot{y} = 0$. As a consequence, C_1 and C_2 can be calculated as

$$C_1 = -\frac{r_2 A_y}{r_1 - r_2} \ , \ C_2 = \frac{r_1 A_y}{r_1 - r_2} \tag{2.21}$$

Hence, the general solution of Eq. (2.20) becomes

$$y = \frac{A_y}{r_1 - r_2} (r_1 e^{r_2 t} - r_2 e^{r_1 t}) \tag{2.22}$$

For case 2, where $c^2 < 4mk$, the roots r_1 and r_2 are complex:

$$\left.\begin{matrix} r_1 \\ r_2 \end{matrix}\right\} = \frac{1}{2m} \left[-c \pm i\sqrt{4mk - c^2} \right] \tag{2.23}$$

The real part of the solution (Eq. 2.20) may be written in the following form

$$y = A_y \ exp\left(-\frac{c}{2m} t\right) cos(\omega_{dv} t) \tag{2.24}$$

where

$$\omega_{dv} = \sqrt{\frac{k}{m} - \left(\frac{c}{2m}\right)^2} \tag{2.25}$$

The solutions for both cases are illustrated in Figure 2.5.
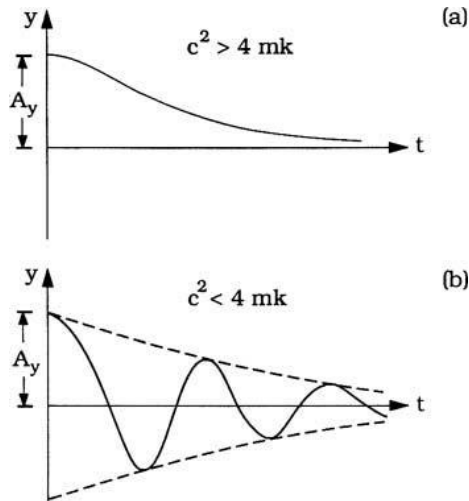
Fig. 2.5. Free vibration with viscous damping, adapted from Sumer [14].

2.2.2. Damping of Fluid

Damping is the ability of a structure to dissipate energy. In this case, the role of damping in flow induced vibration is to limit the vibrations. There are three types of damping: structural damping, material damping and fluid damping. The structural damping is generated by friction, impacting and rubbing between the structures or parts of the structures. The material damping is generated by internal energy dissipation of materials such as rubber, while the latter (i.e., the fluid damping) is generated as the result of relative fluid movement to the vibrating structure. The structural damping has been described in the previous section. This section will, therefore, only focus on the fluid damping description.

A system surrounded by fluid as shown in Figure 2.4 is considered to describe the fluid damping. This system has not only damping due to the structure but also due to the fluid. Under this situation, the structure will be subjected to a hydrodynamic force F. Therefore, the equation of motion will be

$$m\,\ddot{y} + c\dot{y} + ky = F \tag{2.26}$$

in which F is the Morison force per unit length and formulated as

$$F = \frac{1}{2}\rho C_D D(-\dot{y})|-\dot{y}| + \rho C_m A(-\ddot{y}) \tag{2.27}$$

The second term on the right hand side, $\rho C_m A(-\ddot{y})$, may be written in the form $(-m'\ddot{y})$, in which m' is the hydrodynamic mass per unit length. Therefore, Eq. (2.26) becomes

$$(m + m')\ddot{y} + c\dot{y} + \frac{1}{2}\rho C_D D|\dot{y}|\dot{y} + ky = 0 \tag{2.28}$$

From Eq. (2.28), it can be seen that the system has an additional mass m' and resistance force $\frac{1}{2}\rho C_D D|\dot{y}|\dot{y}$. These changes will obviously affect the total damping. The solution of Eq. (2.28) is

$$y = A_y \, exp(-\zeta\omega_d t)cos(\omega_d t) \tag{2.29}$$

in which ζ and ω_d are the total damping factor and damping angular frequency respectively, and ω_d is formulated

$$\omega_d = \omega_n\left(1 - \zeta^2\right)^{0.5} \tag{2.30}$$

where

$$\omega_n = \sqrt{\frac{k}{m+m\prime}} \quad and \quad \zeta = \frac{c}{2m\omega_d} \qquad (2.31)$$

ω_n is called the undamped natural angular frequency. Since ζ contribution is normally small, Eq. (2.30) can then be written as

$$\omega_d = \omega_n\left(1 - \zeta^2\right)^{0.5} \cong \omega_n \qquad (2.32)$$

The natural frequency of the structure, f_n is formulated as

$$f_n = \frac{\omega_n}{2\pi} = \frac{1}{2\pi}\sqrt{\frac{k}{m+m\prime}} \qquad (2.33)$$

The total damping ratio, ζ, consists of the structural damping component (ζ_s) and fluid damping component (ζ_f) and is formulated as

$$\zeta = \zeta_s + \zeta_f \qquad (2.34)$$

$$\zeta_s = \frac{c}{2(m+m\prime)\omega_d} \qquad (2.35)$$

$$\zeta_f = \frac{\rho D^2}{4\pi(m+m\prime)}\frac{8}{3}C_D\frac{A}{D} \qquad (2.36)$$

2.2.3. Cross-Flow and In-Line Vibrations of Cylindrical Structure

Vibrations of structure emerge as the result of periodic variations in the force components due to the vortex shedding. The vibrations can be differentiated into cross-flow and in-line vibrations. The cross-flow vibration is caused by the lift force whilst the in-line one is caused by the drag force. Both vibrations are commonly called the vortex-induced vibrations.

Cyinder

Cross-flow
Vibration

Fluid Flow

Fluid Flow

In-line
Vibration
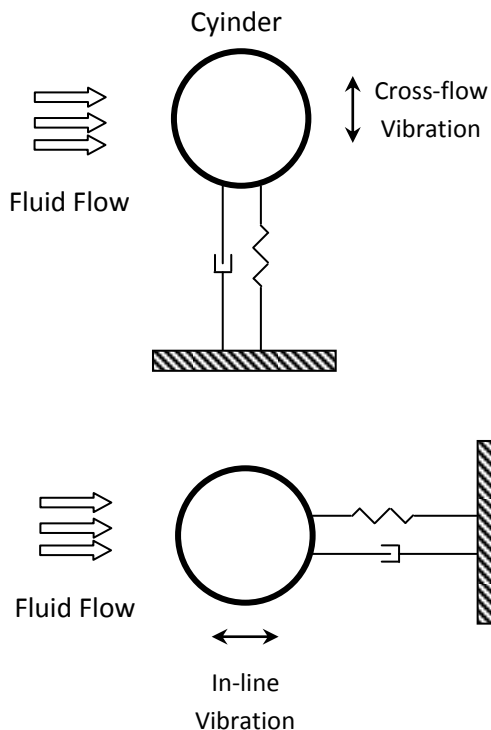
Fig. 2.6. Defenition sketch of vortex-induced vibrations.

The best description of the cross-flow vibrations was carried out by Feng [6]. He mounted a circular cylinder with one degree of freedom and exposed it to an increased air flow in small increments starting from zero. The vortex shedding frequency (f_v), the vibration frequency (f), the amplitude of vibration (A) and also the phase angle (φ), which is the phase difference between the cylinder vibration and the lift force, were measured in his experiment. The set up and the plots obtained from his experiment are depicted in Figures 2.7 and 2.8 respectively.
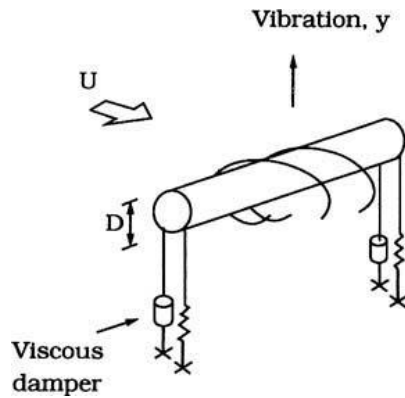
Fig. 2.7. Feng's experimental set up, adapted from Feng [6].

From Figure 2.8a, it can be seen that the vortex shedding frequency, f_v, follows the stationary-cylinder Strouhal frequency, which is represented as dashed reference line, until the reduced velocity, V_r, reaches the value of 5. When the flow speed increases, f_v does not follow the Strouhal frequency, in fact it begins to follow the natural frequency, f_n, of the system, which is represented by the full horizontal line $f/f_n = 1$. This situation takes place at the range of $5 < V_r < 7$.

It can be concluded that in the range of $5 < V_r < 7$, the vortex shedding frequency is locked into the natural frequency of the system. This is known as the ''lock-in'' phenomenon. At this range, f_v, f_n and f have the same values, therefore, the lift force oscillates with the cylinder motion resulting in large vibration amplitudes.

For $V_r > 7$, the shedding frequency suddenly unlocks and jumps to assume its Strouhal value again. This occurs around $V_r = 7.3$. Moreover, the vibration still occurs at the natural frequency, thereby reducing the vibration amplitude as shown in Figure 2.8b. This is caused only by the vortex shedding without the motion of the cylinder.
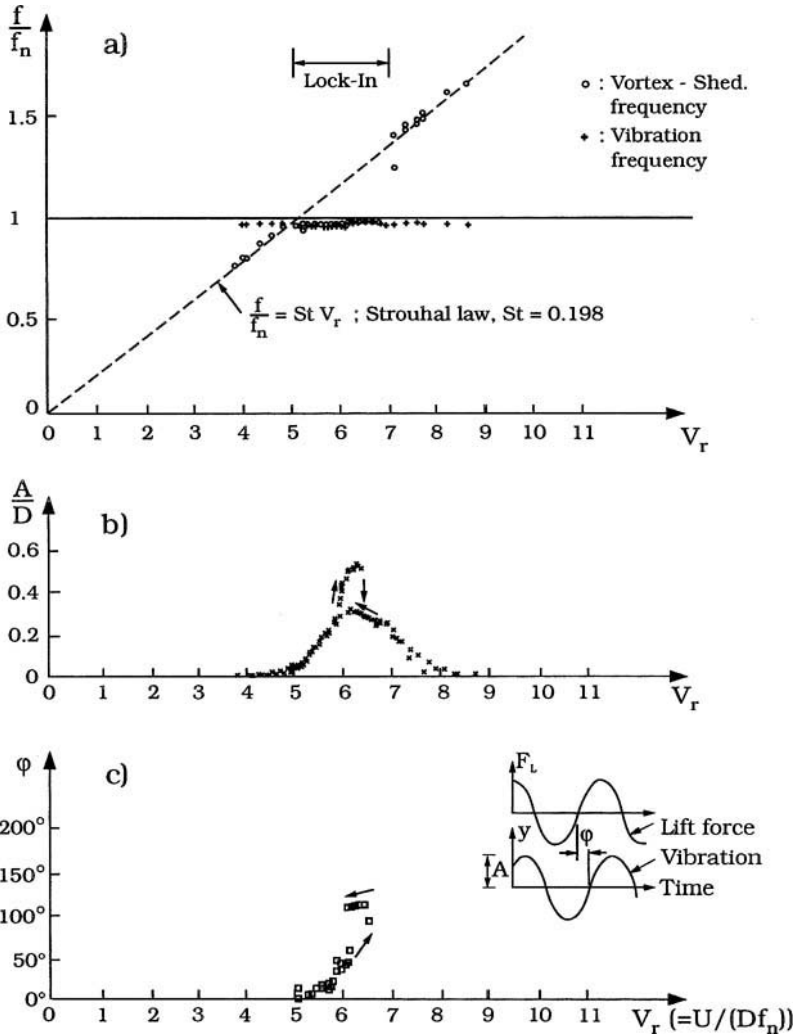
Figure. 2.8. Feng's experiment responses, adapted from Feng [6].

The in-line vibration of a structure is caused by the oscillating drag force and can be differentiated into three kinds represented by the range of the reduced velocity, V_r. First, at the range of $1 \leq V_r \leq 2.5$, which is called the first instability region. Second, at the range of $2.5 \leq V_r \leq 4$, the so-called second instability region. The last occurs at higher flow velocities where the cross-flow vibrations are observed. The first two kinds of the in-line vibrations are shown in Figure 2.9.
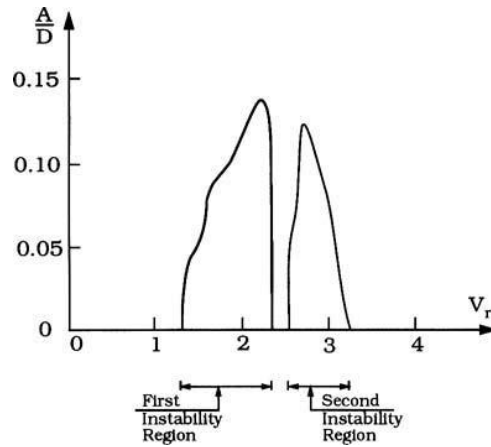
Fig. 2.9. In-line vibrations at Re = 6 x 10^4, adapted from Sumer [14].

The first instability region in-line vibrations are caused by the combination of the normal vortex shedding and the symmetric vortex shedding due to in-line relative motion of the cylinder to that of the fluid. This vortex shedding creates a flow where the in-line force oscillates with a frequency three times of the Strouhal frequency. Consequently, when this frequency has the same value or close to that of natural frequency of the system, the cylinder will start to vibrate. The velocity increases even further, the second instability will occur when the in-line force oscillates with a frequency two times of the Strouhal frequency. Hence, the large amplitude in-line vibrations will occur again when the in-line frequency becomes equal to natural frequency of the system, f_n.

3 COMPUTATIONAL FLUID DYNAMICS

3.1. Introduction

Computational fluid dynamics, usually abbreviated as CFD, is a computer based simulation or numerical modeling of fluid mechanics to solve and analyze problems related to fluid flows, heat transfer and associated phenomena such as chemical reactions. CFD provides a wide range application for many industrial and non-industrial areas. CFD is a very powerful technique regarding the simulation of fluid flows.

The application of CFD began in 1960's when the aerospace industry has integrated CFD techniques into the design, R&D and manufacturing of aircrafts and jet engines [7]. CFD codes are being accepted as design tools by many industrial users. Today, many industrials, for instance, ship industry, power plant, machinery, electronic engineering, chemical process, marine engineering and environmental engineering use CFD as a one of the best design tools.

Unlike the model testing facility or experimental laboratory, in CFD simulations there is no need for a big facility. Furthermore, CFD also offers no capacity limit, no model scale limit and cost and schedule efficiency. Indeed, the advantages by using CFD compared to experiment-based approaches can be concluded as follow:

  a. Ability to assess a system that controlles experiments is difficult or impossible to perform (very large system).
  b. Ability to assess a system under hazardous conditions (e.g. safety study and accident investigation).
  c. Gives unlimited detail level of results.

This chapter describes basic theories and information of fluid dynamics and CFD. Given theories and information are delivered in brief and general. For more detail, readers are recommended to refer to the related sources.

3.1.1. Conservation Laws of Fluid Motion

As mentioned in the previous section, CFD is the science of predicting fluid flow, heat and mass transfer, chemical reactions and other related phenomena. The CFD problems are stated in a set of mathematical equations and are solved numerically. These set of mathematical equations are based on the conservation laws of fluid motion, which are conservation of mass, conservation of momentum, conservation of energy and etc. For CFD problems related to fluid flow, the set of mathematical equations are based on the conservation of mass and momentum.

A. <u>Conservation of Mass</u>

The mass conservation theory states that the mass will remain constant over time in a closed system. This means that the quantity of mass will not change and, the quantity is conserved.

The mass conservation equation, also called the continuity equation can be written as:

$$\frac{\partial \rho}{\partial t} + \frac{\partial (\rho u)}{\partial x} + \frac{\partial (\rho v)}{\partial y} + \frac{\partial (\rho w)}{\partial z} = S_m \tag{3.1}$$

Equation (3.1) is the general form of the mass conservation equation and is valid for incompressible as well as compressible flows. The source S_m is the mass added the system and any user-defined sources. The density of the fluid is ρ and the flow of mass in x, y and z direction is *u*, *v* and *w*.

B. <u>Conservation of Momentum</u>

The conservation of momentum is originally expressed in Newton's second law. Like the velocity, momentum is a vector quantity as well as a magnitude. Momentum is also a conserved quality, meaning that for a closed system, the total momentum will not change as long as there is no external force.

Newton's second law also states that the rate of momentum change of a fluid particle equals the sum of the forces on the particle. We can differentiate the rate of momentum change for x, y and z direction.

$$\rho \frac{Du}{Dt} \qquad \rho \frac{Dv}{Dt} \qquad \rho \frac{Dw}{Dt} \tag{3.2}$$

The momentum conservation equation for x, y and z direction can be written as follows:

$$\rho \frac{Du}{Dt} = \frac{\partial (-p + \tau_{xx})}{\partial x} + \frac{\partial \tau_{yx}}{\partial y} + \frac{\partial \tau_{zx}}{\partial z} + S_{mx} \tag{3.3}$$

$$\rho \frac{Dv}{Dt} = \frac{\partial \tau_{xy}}{\partial x} + \frac{\partial (-p + \tau_{yy})}{\partial y} + \frac{\partial \tau_{zy}}{\partial z} + S_{my} \tag{3.4}$$

$$\rho \frac{Dw}{Dt} = \frac{\partial \tau_{xz}}{\partial x} + \frac{\partial \tau_{yz}}{\partial y} + \frac{\partial (-p + \tau_{zz})}{\partial z} + S_{mz} \tag{3.5}$$

The source S_m is defined as contribution to the body forces in the total force per unit volume on the fluid. The pressure is a normal stress, is denoted p, whilst the viscous stresses are denoted by τ.

3.1.2. General Transport Equation

To derive the transport equation of viscous and incompressible fluids, the Navier-Stokes equation is used. For a Newtonian fluid, which stress versus strain rate curve is linear, the Navier-Stokes equation for x, y and z direction is defined as follows:

$$\rho \frac{Du}{Dt} = -\frac{\partial p}{\partial x} + \frac{\partial}{\partial x} \left[2\mu \frac{\partial u}{\partial x} + \lambda \, div \, \mathbf{u} \right] + \frac{\partial}{\partial y} \left[\mu \left(\frac{\partial u}{\partial y} + \frac{\partial v}{\partial x} \right) \right] + \frac{\partial}{\partial z} \left[\mu \left(\frac{\partial u}{\partial z} + \frac{\partial w}{\partial x} \right) \right] + S_{Mx}$$
$$\tag{3.6}$$

$$\rho \frac{Dv}{Dt} = -\frac{\partial p}{\partial y} + \frac{\partial}{\partial x} \left[\mu \left(\frac{\partial u}{\partial y} + \frac{\partial v}{\partial x} \right) \right] + \frac{\partial}{\partial y} \left[2\mu \frac{\partial v}{\partial y} + \lambda \, div \, \mathbf{u} \right] + \frac{\partial}{\partial z} \left[\mu \left(\frac{\partial v}{\partial z} + \frac{\partial w}{\partial y} \right) \right] + S_{My}$$

$$\tag{3.7}$$

$$\rho \frac{Dw}{Dt} = -\frac{\partial p}{\partial z} + \frac{\partial}{\partial x} \left[\mu \left(\frac{\partial u}{\partial z} + \frac{\partial w}{\partial x} \right) \right] + \frac{\partial}{\partial y} \left[\mu \left(\frac{\partial v}{\partial z} + \frac{\partial w}{\partial y} \right) \right] + \frac{\partial}{\partial z} \left[2\mu \frac{\partial w}{\partial z} + \lambda \, div \, \mathbf{u} \right] + S_{Mz}$$
$$\tag{3.8}$$

And the transport equation is formulated as:

$$\frac{\partial (\rho \phi)}{\partial t} + \text{div}(\rho \phi \mathbf{u}) = \text{div}(\Gamma \, grad \, \phi) + S_\phi \tag{3.9}$$

Lamda (λ) is the dynamic viscosity, which relates stresses to linear deformation and μ is the second viscosity which relates stresses to the volumetric deformation. The value of a property per unit mass is expressed with ϕ.

Equation (3.9) consists of various transport processes, first is the rate of change term or usually called the unsteady term (first term on the left side), second is the convective term (second term on the left side), third is the diffusion term (first term on the right) and fourth is source term (last term). In other words, the rate of increase of ϕ of fluid element plus the net rate of flow of ϕ out of fluid element is equal to the rate of increase of ϕ due to diffusion plus the rate of increase of ϕ due to sources.

3.2.   Methodology of CFD

In general, CFD simulations can be distinguished into three main stages, which are 1) pre-processor, 2) simulator or solver and 3) post-processor.

At the processing stage the geometry of the problem is defined as the solution domain and the fluid volume is divided into discrete cells (the mesh). We also need to define the physical modeling, parameter chemical phenomena, fluid properties and boundary conditions of the problem.

The second stage is the solver. At this stage, the fluid flow problem is solved by using numerical methods either finite difference method (FDM), finite element method (FEM) or finite volume method (FVM).

The last stage is the post-processor. The post-processor is preformed for the analysis and visualization of the resulting solution. Many CFD packages are equipped with versatile data visualization tools, for instance domain geometry and grid display, vector plots, 2D and 3D surface plot, particle tracking and soon.
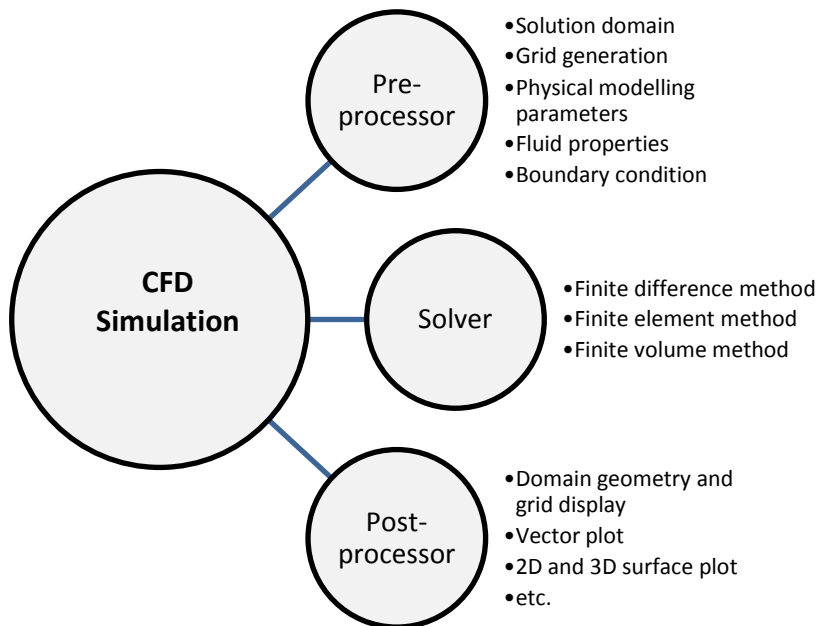
Figure 3.1. Basic concept of CFD simulation methodology.

3.2.1. Pre-processing Stage

As mentioned in the previous section, at this stage we define the flow fluid problem by giving the input in order to get the best solution of our problem. The accuracy of a CFD solution is influenced by many factors, and some of them in this stage.

The pre-processing stage includes:

    a.   Solution domain defining.
    b.   Mesh generation.
    c.   Physical modeling parameters.
    d.   Fluid properties.
    e.   Boundary conditions.

A.   <u>Solution Domain</u>

The solution domain defines the abstract environment where the solution is calculated. The shape of the solution domain can be circular or rectangular. Generally, many simulations use a rectangular box shape as the solution domain as shown in Figure 3.2.
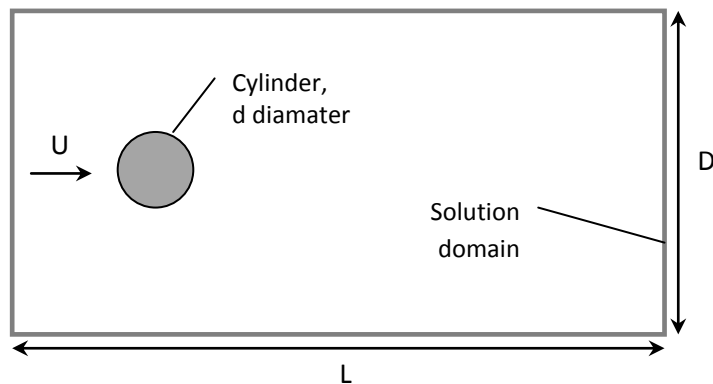
Figure 3.2. A rectangular box solution domain (L x D).

The choice of solution domain shape and size can affect the solution of the problem. The smaller sized of domains need less iterations to solve the problem, in contrast to big domains, which need more time to find the solution.

B.   <u>Mesh Generation</u>

After the solution domain has been defined, we shall generate the mesh within the solution domain. The term mesh generation and grid generation is often interchangeably.

By definition, the mesh or grid is defined as the discrete locations at which the variables are to be calculated and to be solved. The grid divides the solution domain into a finite number of sub domains, for instance elements, control volumes etc [7].

Ferziger and Peric [7] divides grids into three types as follow:

a. Structured (regular) grid

    This regular grid consists of groups of grid lines with the property that members of a single group do not cross each other and cross each member of the other groups only once. This is the simplest grid structure since it has only four neighbors for 2D and six neighbors for 3D. Even though it simplifies programming and the algebraic equation system matrix has a regular structure, it can be used only for geometrically simple solution domains.
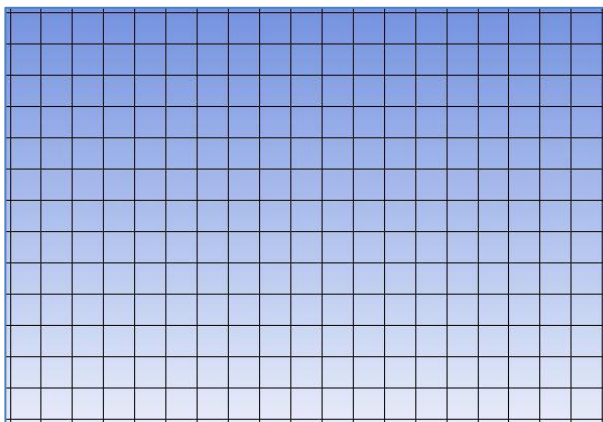
Figure 3.3. A structured grid.

b. Block-Structured grid

    On this type of grid, the solution domain is divided into two or more subdivision. Each subdivision contains of blocks of structured grids and patched together. Special treatment is needed at block interfaces.
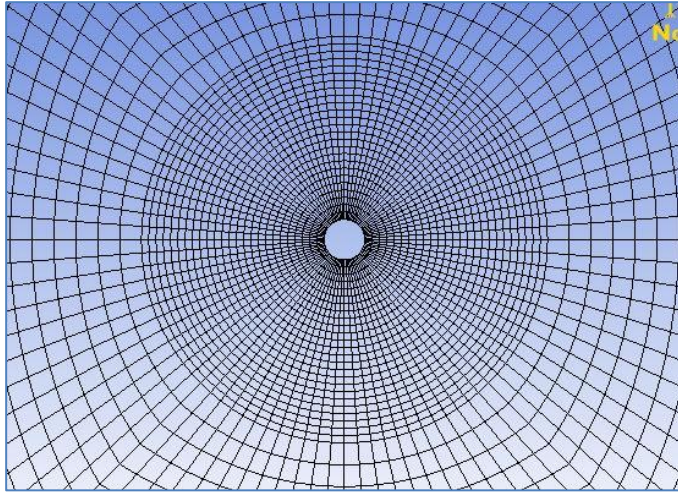
Figure 3.4. Block- structured grid.

c. Unstructured grid

This type of grid can be used for very complex geometries. It can be used for any discretization method, but they are best for finite element and volume methods.

Even though it is very flexible, there is the irregularity of the data structure. Moreover, the solver for the algebraic equation systems is usually slower than for structured grids.
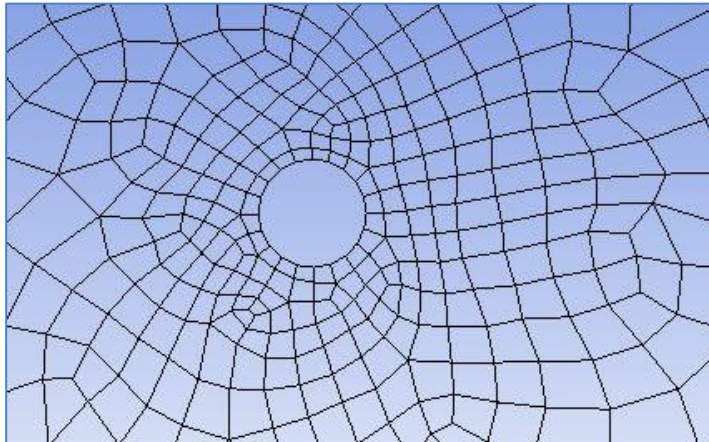
Figure 3.5. Unstructured grid.

C.   **Boundary Condition**

There are several boundary conditions for the discretised equations. Some of them are inlet, outlet, wall, prescribed pressure, symmetry and periodicity [15].

a.   Inlet Boundary Condition

The inlet boundary condition permits flow to enter the solution domain. It can be a velocity inlet, pressure inlet or mass flow inlet.

b.   Outlet Boundary Condition

The outlet boundary condition permits flow to exit the solution domain. It also can be a velocity inlet, pressure inlet or mass flow inlet.

c.   Wall Boundary Condition

The wall boundary condition is the most common condition regarding in confined fluid flow problems, such as flow inside the pipe. The wall boundary condition can be defined for laminar and turbulent flow equations.

d.   Prescribed Pressure Boundary Condition

The prescribed pressure condition is used in condition of external flows around objects, free surface flows, or internal flows with multiple outlets.

e.   Symmetry Boundary Condition

This condition can be classified at a symmetry boundary condition, when there is no flow across the boundary.

f.   Periodic or Cyclic Boundary Condition

Periodic boundary condition is used when the physical geometry and the pattern of the flow have a periodically repeating nature.

3.2.2. Simulation or Solving Stage

In the previous section, it is mentioned that the fluid flow problem is solved by using particular numerical techniques. This technique or method is commonly called the discretization method. The meaning of the discretisation method is that the differential equations are approximated by an algebraic equation system for the variables at some set of discrete location in space and time.

There are three main techniques of discretization method, the finite difference method, the finite element method and the finite volume method. Even though these methods have different approaches, each type of method yields the same solution if the grid is very fine.

A.   Finite Difference Method (FDM)

The Finite Difference Method (FDM) is one of the easiest methods to use, particularly for simple geometries. It can be applied to any grid type, whether structured or unstructured grids.

FDM is very simple and effective on structured grid. It is easy to obtain higher-order schemes on regular grid. On the other hand, it needs special care to enforce the conservation condition. Moreover, for more complex geometry, this method is not appropriate.

B.   Finite Element Method (FEM)

The advantage of FEM is its ability to deal with arbitrary geometries. The domain is broken into unstructured discrete volumes or finite elements. They are usually triangles or quadrilaterals (for 2D) and tetrahedral or hexahedra (for 3D). However, by using unstructured grids, the matrices of the linearized equations are not as well ordered as for structured grids. In conclusion, it is more difficult to find efficient solution methods.

FEM is widely used in structural analysis of solids, but is also applicable to fluids. To ensure a conservative solution, FEM formulations require special care. The FEM equations are multiplied by a weight function before integrated over the entire solution domain. Even though the FEM is much more stable than finite volume method (FVM), it requires more memory than FVM.

C.   Finite Volume Method (FVM)

FVM is a common approach used in CFD codes. Any type of grid can be accommodated by this method, indeed it is suitable for complex geometries. This method divides the solution domain into a finite number of contiguous control volume (CV), and the conservation equations are applied to each CV. The FVM approach requires interpolation and integration, for methods of order higher than second and are more difficult to develop in 3D.

3.3. Turbulent Flows

Turbulent flow can be defined as a chaotic, fluctuating and randomly condition of flow, i.e. velocity fields. These fluctuations mix transported quantities such as momentum, energy, and species concentration, and cause the transported quantities to fluctuate as well. Turbulence is a time-dependent process. In this flow, the solution of the transport equation is difficult to solve.

There are many methods that can be used to predict turbulence flow. Some of them are DNS (direct numerical solution), RANS (Reynolds averaged Navier-Stokes), and LES (large eddy simulation).

3.3.1. Direct Numerical Solution (DNS)

DNS is a method to predict the turbulence flow in which the Navier-Stokes equations are numerically solved without averaging. This means that all the turbulent motions in the flow are resolved.

DNS is a useful tool in fundamental research in turbulence, but it is only possible to be performed at low Reynolds number due to the high number of operations as the number of mesh points is equal to Re^3[1]. Therefore, the computational cost of DNS is very high even at low Re. This is due to the limitation of the processing speed and the memory of the computer.

3.3.2. Large Eddy Simulations (LES)

The principal operation of LES is low-pass filtering. This means that the small scales of the transport equation solution are taking out by apply the low-pass filtering. On the whole, it reduces the computational cost of the simulation. The reason is that only the large eddies which contain most of the energy are resolved.
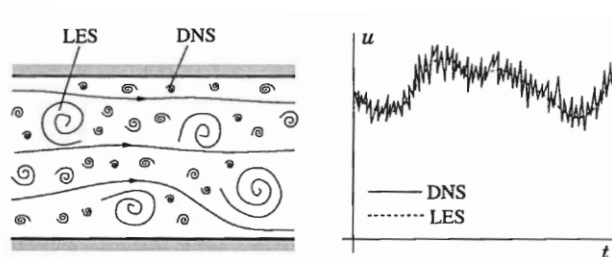
Figure 3.6. Schematic representation of turbulent motion and time dependent of a velocity component, adapted from Ferziger and Peric [1].

3.3.3. Reynolds Averaged Navier-Stokes (RANS)

RANS equations are the time-averaged equations of motion of fluid flow. They govern the transport of the averaged flow quantities, with the complete range of the turbulent scales being modeled. Therefore, it greatly reduces the required computational effort and resources and is widely adopted for practical engineering applications.

Two of the most popular models of the RANS are the k-ε model and k-ω model. The k-ε was proposed for first time by Launder and Spalding [10]. Robustness, economy and reasonable accuracy for a wide range of turbulent flows become its popularity. The k-ω model is based on the Wilcox [16] k-ω model. This model is based on model transport equations for the turbulence kinetic energy (k) and the specific dissipation rate (ω).

3.4. Solution Algorithms for Pressure-Velocity Coupling Equation

To solve the pressure-velocity coupling equation, we need particular numerical procedures called the solution algorithms. There are many algorithms that have been developed, for instance SIMPLE, SIMPLEC, SIMPLER and PISO. These solution algorithms are also called the projection methods.

3.4.1. SIMPLE Algorithm

SIMPLE is an acronym for Semi-Implicit Method for Pressure Linked Equations. It is widely used to solve the Navier-Stokes equations and extensively used by many researchers to solve different kinds of fluid flow and heat transfer problems.

This method considers two-dimensional laminar steady flow equations in Cartesian co-ordinate. The principal of this method is that a pressure field ($p*$) is guessed to solve the discretized momentum equations and resulting velocity component $u*$ and $v*$. Furthermore, the correction pressure (p') is introduced as the difference between the correct pressure (p) and guessed $p*$. In summary, it will yield the correct velocity field (u and v) and continuity will be satisfied.

3.4.2. SIMPLER Algorithm

SIMPLER is a revised and improved method of SIMPLE. Note that R is stand for revised. This method uses the SIMPLE's velocity correction to obtain the velocity fields.

3.4.3. SIMPLEC Algorithm

SIMPLEC has the same steps as SIMPLE algorithm. The difference is that momentum equations are manipulated so that the velocity correction equations of SIMPLEC omit the terms that are less significant than those omitted in SIMPLE.

3.4.4.   PISO

Pressure implicit with splitting operators, usually abbreviated as PISO, is a pressure-velocity procedure developed originally for the non-iterative computation of unsteady flow [15]. This procedure has been successfully adapted for the iterative solution of steady state problems. PISO consists of one predictor step and two corrector step.

At the predictor step, a guessed pressure (p) field is used to solved the discretized momentum equation to give the velocity component (u and v). Furthermore, the first corrector step of SIMPLE is used to give a velocity field which satisfies the discretized continuity equation. Finally, second corrector step is applied to enhance the SIMPLE procedure to obtain the second pressure correction field.

4 VALIDATION OF THE CFD SIMULATIONS

This chapter describes the validation of the two dimensional steady flow simulation of flow around a cylindrical structure using ANSYS Fluent. There are two main parts in this chapter, first is the determination of the domain and grid type. Second is the validation part. Many previous experiment results are given for validation and comparison with the simulation results.

4.1. The Determination of Domain and Grid Type

The most important and crucial stage in the CFD simulation is the grids generation. Moreover, the success of the CFD simulation depends on quality of the mesh. In this section, several types of domains and grids have been generated and the best mesh quality will be chosen for further simulation.

For problem of the flow around cylindrical structure, the possibilities of the domain shape could be a circular, square or rectangular.

4.1.1. The Evaluation of the Grid Quality

The evaluations of the grid quality are based on the observation and criteria given by ANSYS-Fluent [1]. Some of them are:

A. Skewness
One of the major quality measures for a mesh is the skewness. It determines how close to ideal a face or a cell is. It is expressed by values in a range between $0 - 1$ as shown in Table 4.1. Highly skewed faces and cells are unacceptable because the equations being solved assume that the cells are relatively equilateral/equiangular. Figure 4.1 shows the ideal and skewed triangles and quadrilaterals.

Table 4.1. Value of Skewness

Value of Skewness	Cell Quality
1	Degenerate
0.9 - <1	Bad (sliver)
0.75 – 0.9	Poor
0.5 – 0.75	Fair
0.25 – 0.5	Good
>0 – 0.25	Excellent
0	Equilateral

Equilateral Triangle   Highly Skewed Triangle

Equilateral Quad   Highly Skewed Quad
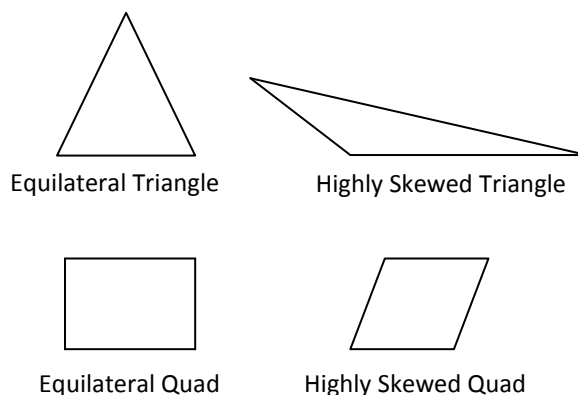
Figure 4.1. Ideal and skewed triangles and quadrilaterals.

B. Element Quality
    The element quality is expressed by a value in the range of 0 to 1. A value of 1 indicates a perfect cube or square while a value of 0 indicates that the element has a zero or negative value.

C. Orthogonal Quality
    The range for orthogonal quality is $0 – 1$, where a value of 0 is worst and 1 is the best.

D. Aspect Ratio
    Aspect ratio is differentiated into two types which are the triangles and quadrilaterals. Both are expressed by a value of number start from 1. A value of 1 indicates the best shape of an equilateral triangles or a square. Figure 4.2 shows the aspect ratio for triangles and quadrilaterals.
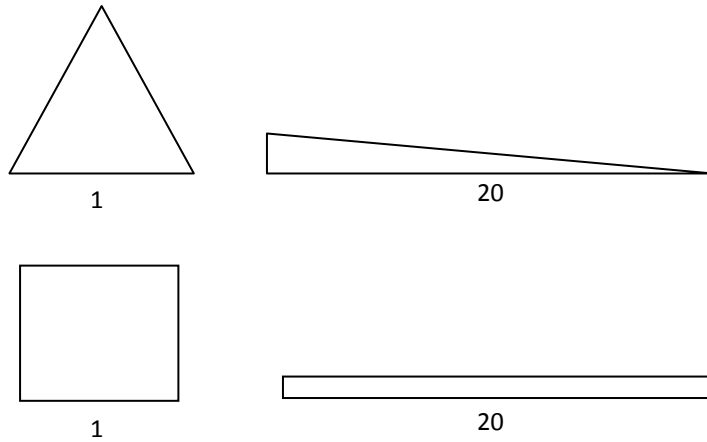
Figure 4.2. Aspect ratio for triangles and quadrilaterals

E.   Jacobian Ratio

The Jacobian ratio is computed and tested for all elements and expressed by a value of number start from 1. An illustration for different values of Jacobian ratio is shown in Figure 4.3.
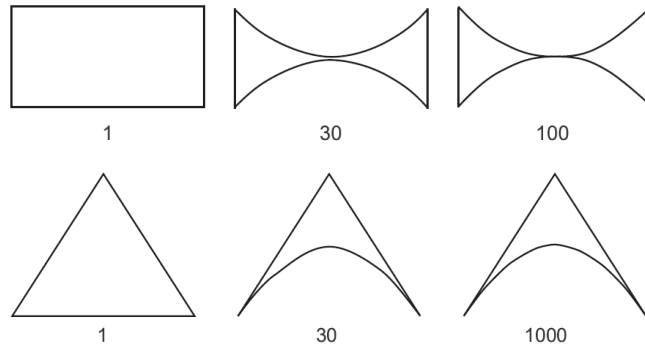
Figure 4.3. Jacobian ratio for triangles and quadrilaterals

Several domains have been generated and compared in order to obtain the best option. Generated domains and grids types are differentiated into four types. Each type will be presented and the evaluation of the grid quality is presented in tabulation form as shown in Table 4.2.

A.   Circular Domain with Quadrilateral Grids

The circular domain has a uniform grid distribution along the geometry. It is the easiest domain to be generated. The cylinder wall is located at the center of the domain with D diameter. Figure 4.4 shows the typical circular domain with 1 m of cylinder diameter and 64D of domain diameter.
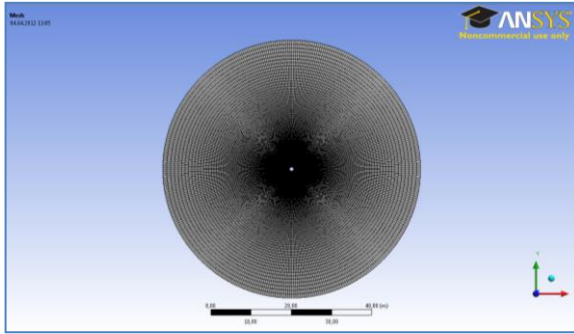
Figure 4.4. Circular domain with quadrilateral grids.

This domain is divided into 192 circumferential divisions and 192 radial divisions and results in 73.728 elements. However, we can observe that the grid quality is not uniformly distributed along the geometry face, especially for area close to the cylinder wall (center). Detail view on Figure 4.5 indicates that the elements around the cylinder wall have variation in grid quality.
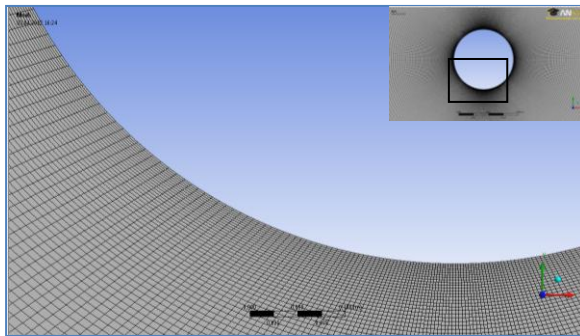
Figure 4.5. Detail view of circular domain grids.

B.   Square Domain with Quadrilateral Grids

This domain uses a square shape with dimension 60D length and 60D width. The cylinder is located at the middle of the geometry as indicated in Figure 4.6.
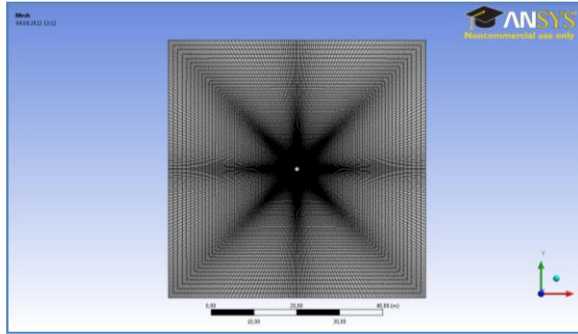
Figure 4.6. Square domain with quadrilateral grids.

Domain face is divided into 8 equal parts and each inner line is divided into 160 divisions. Furthermore, cylinder wall is divided into 400 circumferential divisions. Hence, 64.000 elements are created. In spite of we divide the domain into 8 equal parts, the grid distribution is not uniformly distributed along the domain face.

C.   Rectangular Domain with Quadrilateral Grids

This domain has 50D x 30D dimension. The cylinder position in x-direction is located at 1/5 of the length and for the y-direction is ½ of the width as indicated in Figure 4.7.

The establishment of the grid uses an automatic feature by Fluent called mapped face meshing with 100% relevancy. The grids distribution is indicated in Figure 4.7. Even though this method is the simplest and the easiest way to create the grids, in contrast it produces low level of the grid quality as indicated in Figure 4.8.
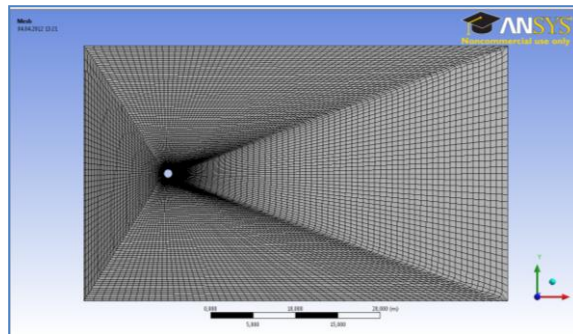
Figure 4.7. Rectangular domain with quadrilateral grids.
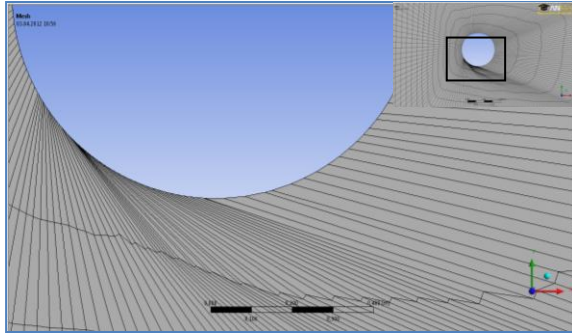
Figure 4.8. Detail view of the rectangular domain grids.

D.   Rectangular Domain with Smooth Quadrilateral Grids

This domain has 60D x 90D dimension. The domain face is divided into 10 divisions and has a wireframe configuration as indicated in Figure 4.9. This wireframe arrangement leads the smooth transition between two adjacent faces and generates uniform grid distribution as indicated in Figure 4.10 and 4.11. Finer grids are needed in area close to the wall in order to obtain precise results.
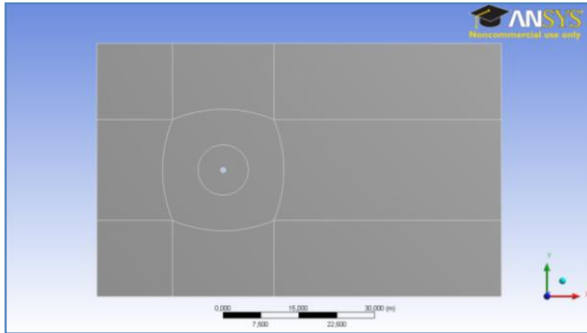
Figure 4.9. Wireframe arrangement of rectangular domain.
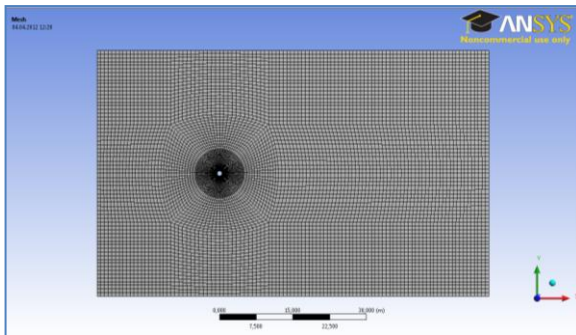
Figure 4.10. Rectangular domain with smooth quadrilateral grids.
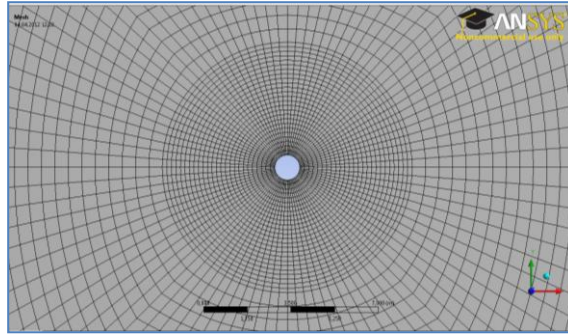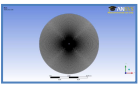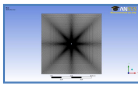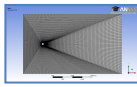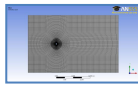
Figure 4.11. Detail view of the smooth grids close to the cylinder wall.

4.1.2. The Result of the Evaluation of the Grid Quality

By assessing the grid quality measurements as explained in the previous section, a tabulation of grid quality for different type of domains is given in Table 4.2. The table indicates the values of different grid quality criteria for each domain.

Table 4.2. Grid quality measurements.

Criteria	Circular Domain			Square Domain			Ractangular Domain			Smooth Rectangular		
	Min	Max	Avrg	Min	Max	Avrg	Min	Max	Avrg	Min	Max	Avrg
Skewness	0.005	0.265	0.066	3.604	0.500	0.190	2.922	0.964	0.371	1.3E-10	0.267	0.041
Element Quality	0.243	0.994	0.807	0.306	0.996	0.697	-0.001	0.993	0.503	0.349	0.999	0.923
Orthogonal Quality	0.915	0.999	0.989	0.702	0.999	0.932	3.298	0.999	0.769	0.918	1	0.994
Aspect Ratio	1.002	7.931	1.848	1.002	5.010	2.107	1.002	123.63	3.983	1	4.660	1.283
Jacobian Ratio	1.002	1.033	1.025	1.004	1.040	1.029	1.002	31.348	1.132	1	1.36	1.038

Min = Minimum; Max = Maximum; Avrg = Average

Referring to the values given in Table 4.2, it can be concluded that the best domain and grid quality is the rectangular domain with smooth quadrilateral grid. Therefore, this domain will be used for further simulations.

4.1.3. The Grid Independency Study

The objective of the grid independency study is to precisely determine the grid size to produce an accurate result. The grid independency is considered to be achieved when the solution is not affected anymore by the size of the grid.

In this study, 2-dimensional steady flow at Re = 40 simulations has been carried out for 8 different sizes of grids. It is noted that the simulations use a rectangular domain with smooth grids as proposed in the previous section. The first simulation uses 2 384 elements and yields Cd was equal to 1.431. The second simulation uses 9 728 elements (308% higher than first simulation) increases Cd by 10.83% which was 1.586. However, increasing the element number by 125% in fifth simulation yields a very small change to the Cd, which only rises up to 0.1%. The results of the 8 different grid sizes are given in Table 4.3. Figure 4.12 shows the result of the grid independence study.

Table 4.3. Result of the different grid size simulation at Re = 40.

Simulation Number	No. Of Element	Cd
S1	2 384	1.430
S2	9 728	1.586
S3	21 744	1.595
S4	38 912	1.601
S5	87 552	1.602
S6	136 620	1.602
S7	196 560	1.602
S8	442 908	1.606

As indicated in Figure 4.12, solution starts to converge at the 4th simulation which the grids number is equal to 38.912. In conclusion, the minimum number of grids in order to produce an accurate solution is 38.912.
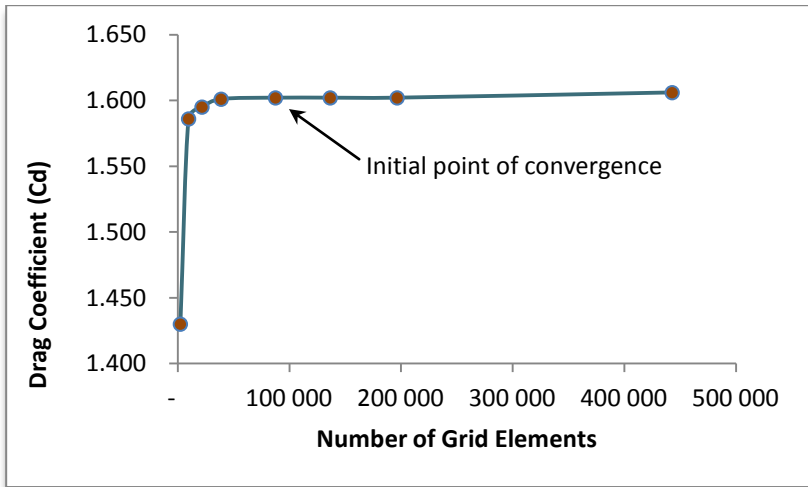
Figure 4.12. Result of the grid independence study.

4.2. The Validations of the Results

This section describes the validation of the CFD simulations by comparing the simulation solutions to the previous studies. The case of simulation is a 2-dimensional case for difference values of Re = 40, 100 and 200.

4.2.1. The Steady Laminar Case at Re = 40

At Re = 40, two-attached recirculating vortices will be formed at the wake region. Apart from the coefficient of drag (Cd), other features will be validated as indicated in Figure 4.13. Linnick and Fasel [5] did an experiment of a steady uniform flow past a circular cylinder for Re was equal to 40. They measured the Cd value, length of recirculation zone (L/D), vortex centre location (a/D,b/2D) and the separation angle (θ). These measurements were also carried out by Herfjor [9] and Berthelsen and Faltinsen [3]. In addition, the measurement of the separation angle (θ) also was conducted by Russel and Wang [13], Xu and Wang [17] and Calhoun [4]. The summary of the measurements is given in Table 4.4.
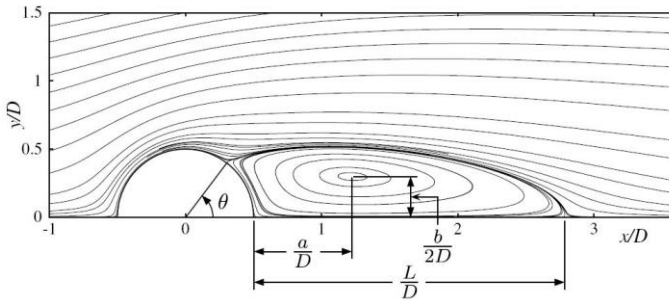
Figure 4.13. Vortice features for Re = 40, adapted from [10].

The simulation is set at Re = 40 and a steady laminar flow condition. The SIMPLE is used as the pressure-velocity coupling scheme and QUICK is used as the momentum spatial discretization. The QUICK scheme will typically be more accurate on structured meshes aligned with the flow direction [2]. Moreover, 3000 iteration is set for the simulation.

The solution is converged at 884 iterations and yields Cd is equal to 1.6002. At this Re value, two identical vortices is formed behind the cylinder wall as indicated in Figure 4.14. Furthermore, the result of the measurement of the vortice features is shown in Table 4.4.

Table 4.4. Vortice features measurements of a steady flow past a circular cylinder for Re = 40.

Experiment by	L/D	a/D	b/D	θ (deg)	Cd
Linnick and Fasel [11]	2.28	0.72	0.6	53.6	1.540
Herfjord [9]	2.25	0.71	0.6	51.2	1.600
Berthelsen and Faltinsen [3]	2.29	0.72	0.6	53.9	1.590
Russel and Wang [13]	2.29	-	-	53.1	1.600
Xu and Wang [17]	2.21	-	-	53.5	1.660
Calhoun [4]	2.18	-	-	54.2	1.620
Present study	**2.27**	**0.73**	**0.6**	**49.5**	**1.600**

Based on the results shown in Table 4.4, it can be concluded that the present value of the simulation for Re = 40 is in a good agreement to the other measurements.
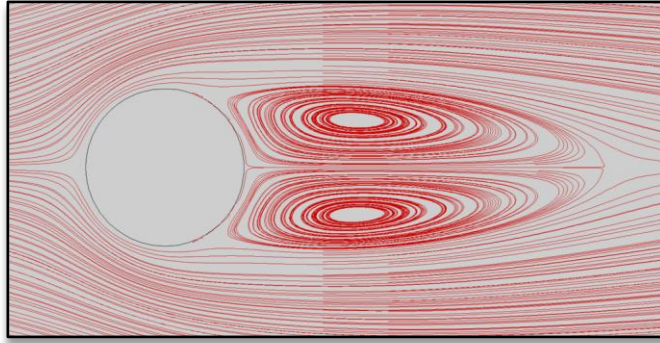
Figure 4.14. Simulation result of two identical vortices at Re = 40.

4.2.2. The Transient (unsteady) Case at Re 100, 200 and 1000

For the 40 < Re < 200, the laminar vortex shedding will be formed behind the cylinder wall as the result of the instability of the wake region. Furthermore, the vortex street experiences the transition from laminar to turbulence and moves toward the cylinder wall as Re is increased in the range 200 < Re < 300. When Re further increases (Re > 300), the wake region behind the cylinder wall becomes completely turbulent. The flow regime at this Re value is described as the subcritical region ($300 < Re < 3.5 \times 10^5$).

In this case, the cylinder is exposed to the transient laminar flow at Re = 100, 200 and 1000. Moreover the cylinder is also exposed to the transient turbulent flow at Re = 200 and 1000. The comparison of the results will be presented. For the transient laminar flow case, the PISO is selected as the pressure-velocity coupling solution, since it gives a stable solution for transient applications [2]. The large eddies simulation (LES) is selected for the turbulent model in modeling the transient turbulent flow case.

To capture the shedding correctly, 25 time steps were chosen in one shedding cycle for St = 0.2 (average estimation for flow past cylinder). In this case, for D = 1 m and U = 1 m/s, the vortex shedding frequency will be 0.2 Hz. Therefore, the time step is equal to 0.2 seconds. Figure 4.15 shows the time history of Cl and Cd at Re 100, 200 and 1000 and the Strouhal frequency for the transient laminar flow case. The transient turbulent flow is shown in Figure 4.16.

The comparison of the Cd and Cl values are given in Table 4.5. It can be seen that the application of the LES turbulent model yields the good agreement with previous studies. This is due to the capability of the LES model to resolve all eddies. On the other hand, the results from the transient laminar case show a wide discrepancy to the other studies. This might be caused by the limitation of the laminar model to resolve the momentum, mass and energy equations that are transported by the large eddies.

Table 4.5. Experimental results of the Cl and Cd at Re 100, 200 and 1000.

Experiment by	Re = 100		Re = 200		Re = 1000	
	Cd	Cl	Cd	Cl	Cd	Cl
Linnick and Fasel [11]	1.34	0.333	1.34	0.69	-	-
Herfjord [9]	1.36	0.34	1.35	0.70	-	-
Berthelsen and Faltinsen [3]	1.38	0.34	1.37	0.70	-	-
Russel and Wang [13]	1.38	0.30	1.29	0.5	-	-
Xu and Wang [17]	1.42	0.34	1.42	0.66	-	-
Calhoun [4]	1.33	0.298	1.17	0.668	-	-
Franke, *et al* [8]	-	-	1.31	0.65	1.47	1.36
Rajani, *et al* [12]	1.335	0.179	1.337	0.424	-	
Present study*	**1.28**	**0.13**	**1.20**	**0.29**	**0.80**	**0.37**
Present study**	**1.42**	**0.38**	**1.29**	**0.48**	**1.40**	**1.22**

  * *Simulation results for the transient laminar flow*

  ** *Simulation results for the transient turbulent flow (LES model)*
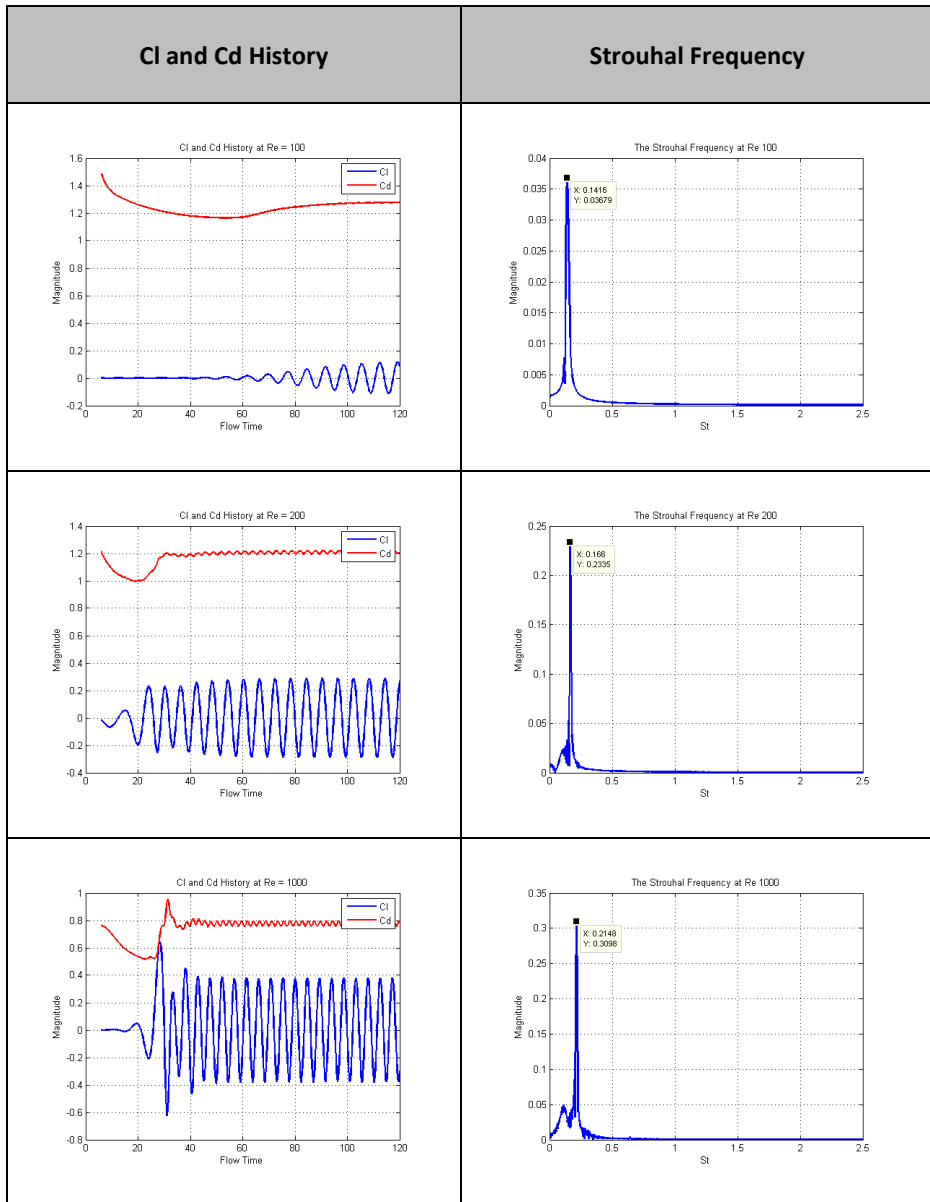
Figure 4.15. The time history of Cl and Cd for transient laminar flow case.

Cl and Cd History	Strouhal Frequency
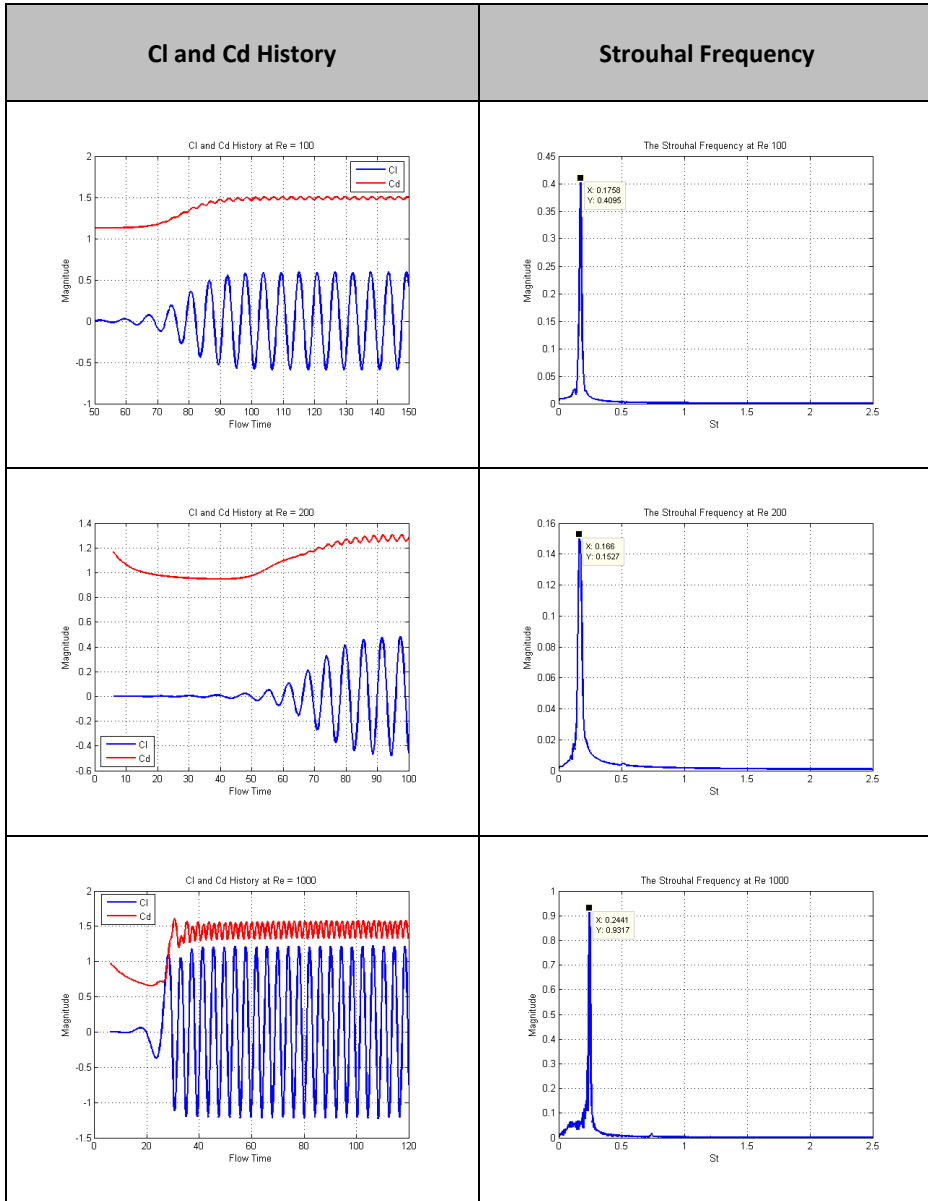
Figure 4.16. The time history of Cl and Cd for transient turbulent flow case (LES).

5 THE VORTEX INDUCED VIBRATION SIMULATIONS

This chapter describes the vortex induced vibrations (VIV) simulations at Re 100, 200 and 1000. To simulate the vibrations of the cylinder due to the flow, the dynamic mesh method is performed and a user defined function (UDF) was introduced to define the motion of the cylinder. To capture the displacement of the cylinder clearly, the cylinder is set to freely vibrate in the cross-flow direction (y direction) by defining the mass per length of the cylinder is set equal to 1 kg, while the natural frequency (f_n) is set equal to 0.2 Hz. There is no structural damping included in the motion of the cylinder, the damping is only provided by the fluid due to the viscosity. The purpose of the VIV simulation is to measure cross-flow displacement of the cylinder due to the flow. In addition, the real vortex shedding frequency (f_v), the vibration frequency (f_{vib}), Strouhal number (St) and the amplitude of the vibration (A) were also calculated.

This chapter is divided into three parts. First, the description of the VIV simulation setup. Secondly, the result of the VIV simulation for Re 100, 200 and 1000. And finally, the discussion of the results will be given on the last part.

5.1. Simulation Setup

In order to obtain the accurate and stable result numerically, some procedures had been applied. The procedures include the choice of the turbulent model, the pressure-velocity coupling scheme and the momentum spatial discretization.

5.1.1. Turbulent Model

In this VIV simulation, the large eddy simulation (LES) is selected to resolve the turbulent flow. LES is able to resolve the large eddies directly, while the small eddies are modeled.

5.1.2. Pressure-Velocity Coupling Scheme

Two schemes have been tested in this VIV simulation. First is the PISO and second is the SIMPLE. Even though the PISO gives a stable solution for transient application of a fixed cylinder (Chapter 4), it produced unstable solution for the freely vibrating cylinder. Here the SIMPLE gives a stable solution.

5.1.3. Momentum Spatial Discretization

The Bounded Central Differencing is set for the momentum spatial discretization scheme. This is the default scheme for LES model and is available only in the pressure-based solver. Other momentum spatial discretization is also tried in this simulation, the QUICK. Although the QUICK scheme will typically be more accurate on structured meshes aligned with the flow direction, it produces an error due to the negative cell volume. This error occurs due to the mesh deformation becomes too large in one time step.

5.2. The Result of the Simulation of the VIV

In Figure 5.1, the displacement history of the freely vibrating cylinder at Re = 100 is shown. The simulation is conducted for 100 second flow time. The vertical axes indicate both the lift coefficient (Cl) and the non-dimensional magnitude of the cylinder displacement (A/D). From the figure, it can be seen that the cylinder response rises few second after the force.
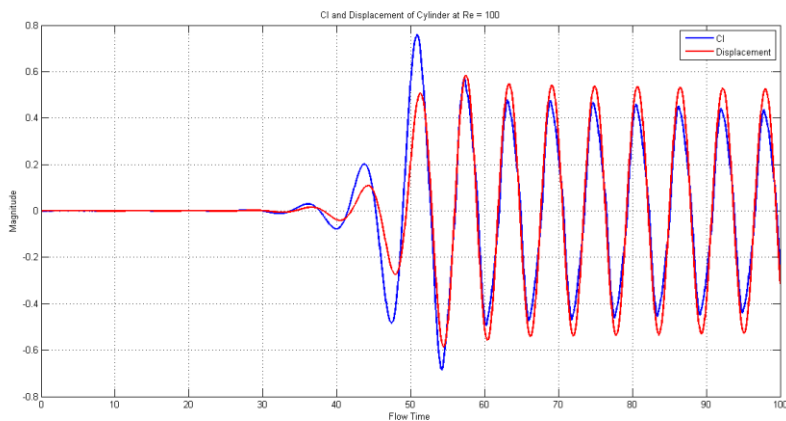
Figure 5.1. Lift coefficient and displacement (A/D) of the cylinder at Re = 100.

The Fast Fourier Transform (FFT) is implemented to calculate the frequencies spectrum of f_v and f_{vib} as indicated in Figure 5.2. The vortex shedding frequency (f_v) has the value of 0.166 Hz whilst the vibration frequency (f_{vib}) is 0.176 Hz. The frequency ratio between f_{vib} and f_n, f_{vib}/f_n is equal to 0.88.
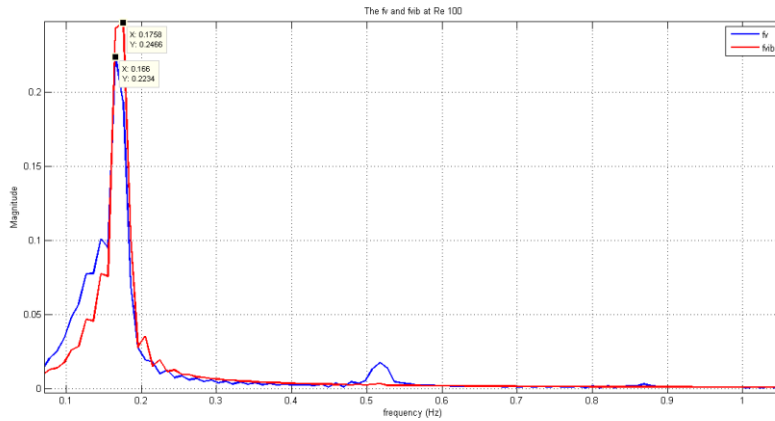
Figure 5.2. Spectrum of CF response frequencies (f_v and f_{vib}) at Re = 100.

The displacement history of the cylinder at Re = 200 is indicated in Figure 5.3. The figure shows that the displacement of the cylinder grows larger than the force.
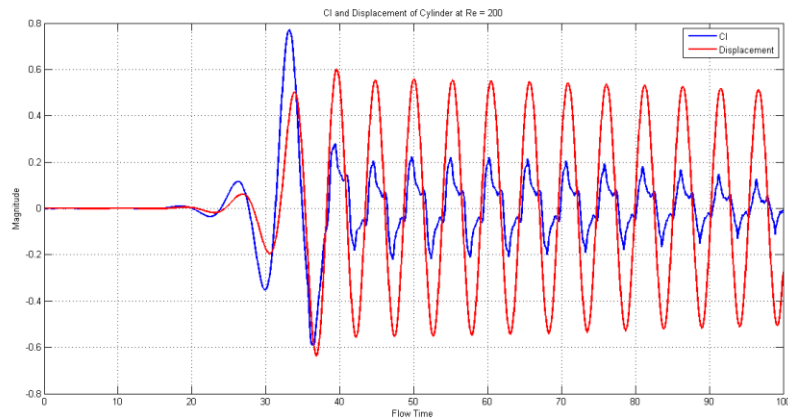
Figure 5.3. Lift coefficient and displacement (A/D) of the cylinder at Re = 200.

The frequencies spectrum at Re = 200 is shown in Figure 5.4. The f_v is equal to 0.186 whilst f_{vib} is equal to 0.195. Therefore the f_{vib}/f_n is equal to 0.98.
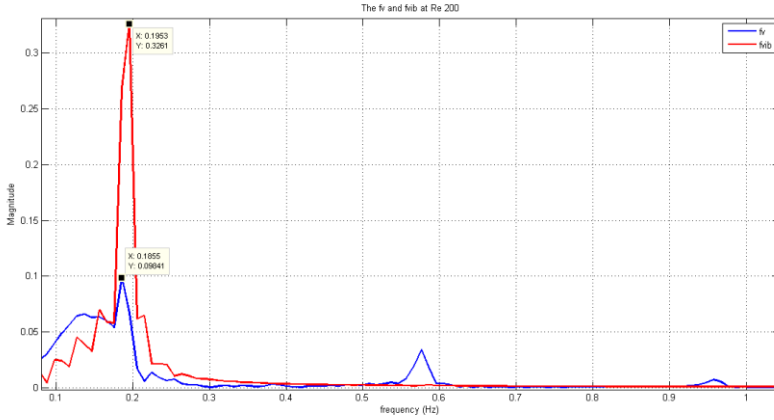
Figure 5.4. Spectrum of CF response frequencies (f_v and f_{vib}) at Re = 200.

Figure 5.5 indicates the displacement history of the cylinder at Re = 1000. In this case the U is set equal to 0.5 m/s. The reason is to maintain the stability of the numerical calculation. As the consequence, the fluid viscosity must be set to 0.0005 kg/m-s. It can be seen from the figure that the magnitude of the displacement is much lower than the displacement for Re 100 and 200.
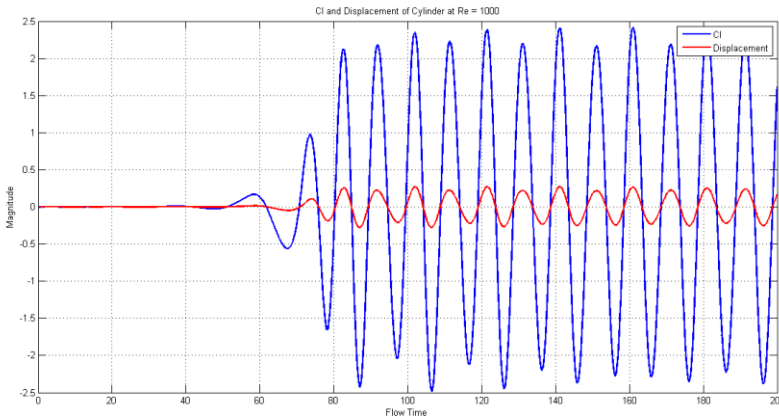
Figure 5.5. Lift coefficient and displacement (A/D) of the cylinder at Re = 1000.

The value of the frequencies shows the same value as indicated in Figure 5.6. Both f_v and f_{vib} have the frequency of 0.103 Hz. This means that ratio of ${f_{vib}}/{f_n}$ is equal to 0.52.
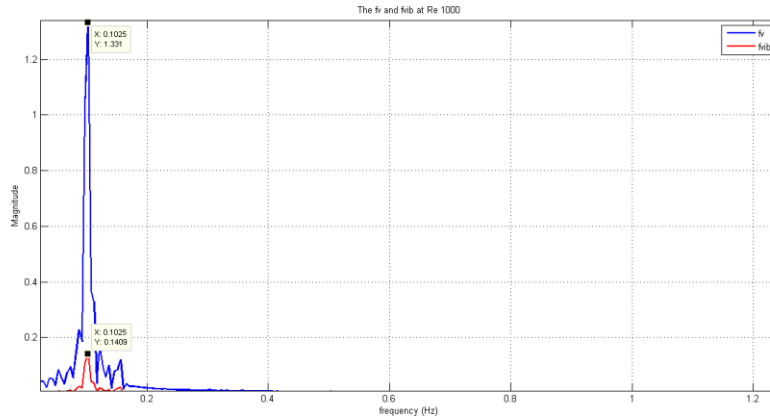
Figure 5.6. Spectrum of CF response frequencies (f_v and f_{vib}) at Re = 1000.

5.3. Discussion

5.3.1. Effect of The Fluid Damping

As mentioned in the previous subchapter, there is no structural damping included in the motion of the cylinder, the damping is only provided by the fluid due to the viscosity. The fluid damping is the result of energy dissipation, as the fluid moves relative to the vibrating structure, the cylinder. The interaction of the cylinder and the fluid produces the additional mass (added mass) and this obviously affects the total damping.

In a vacuum environment, the response of the structure is stationary and no decrement. Indeed, in this case the decrement are exist as we can observe if Figure 5.1 and 5.3. By contrast, at Re 1000 the decrement seems does not exist (Figure 5.5). It is presumably caused by the small effect of the added mass due to the small displacement of the cylinder.

5.3.2. The Displacement of The Cylinder (Cross-Flow Direction)

Table 5.1 indicates the result of the measurements of the VIV simulation at Re 100, 200 and 1000. The value of amplitude is calculated by using the root mean square (RMS) method. The true reduced velocity, $U_{red,true}$, is based on the frequency at which the cylinder is actually vibrating (f_{vib}).

From the table, it can be seen that the magnitude of the dimensionless displacement (A/D) at Re 100 and 200 does not change even though the Re doubles. This is caused by the vibration frequency which for both Re values is quite same. However, there is a significant decrease in the displacement magnitude for Re 1000, which is 55%

decrement. The reason behind this decrement is that the vibration frequency (f_{vib}) quite differs to the value of the natural frequency (f_v) of the cylinder, as indicated in Table 5.1.

Table 5.1. Result of the VIV simulation.

Re	**f_v**	**S_t**	**f_{vib}**	**$U_{red,true}$**	**A/D**	**f_{vib}/S_t**	**f_{vib}/f_n**
100	0.166	0.166	0.176	5.68	0.379	1.06	0.88
200	0.186	0.186	0.195	5.13	0.380	1.05	0.98
1000	0.103	0.206	0.103	4.85	0.172	0.5	0.52

To explain the displacement of the cylinder in cross-flow direction, Figure 2.8 can be referred. From the figure, it can be concluded that the vortex-shedding frequency follows the cylinder's Strouhal frequency until the velocity U_{red} reaches the value of 5. Beyond this point, however, the vortex-shedding frequency begins to follow the natural frequency of the system ($f_{vib}/f_n = 1$) until it reaches $U_{red} = 7$. This phenomenon is known as the 'lock-in' phenomenon. In this range, the vortex-shedding frequency, the vibration frequency and the natural frequency coincide ($f_v = f_{vib} = f_n$). This means that, in this range the lift force (the shedding) oscillates in sympathy with the cylinder motion, results in the largest amplitude. The same thing occurs in this case. The maximum displacement happened at $U_{red,true} = 5.13$. At this point, the value of f_v, f_{vib} and f_n relatively have the same value. By contrast, the smallest displacement happens at $U_{red,true} = 4.85$, which have the f_v and f_{vib} 50% smaller than f_n.

5.3.3. The Displacement Initiation

The time required to initiate the displacement of the cylinder is different for each case. For Re 100, the initiation of the displacement starts at the flow time was equal to 32.2 second (Figure 5.1), for Re 200 the initiation starts at the flow time was equal to 23.3 second (Figure 5.3), whilst for Re 1000 the initiation starts after 68 second (Figure 5.5). These initiations are strongly associate with the frequency of the vibration (f_{vib}). The closest f_{vib} to the f_n value, the faster the displacement initiation. From the Table 5.1, at Re 200 the ratio of f_{vib}/f_n is 0.98, which means that the value of f_{vib} is close to the f_n of the cylinder. Figure 5.7 shows the development of the displacement of the cylinder as a function of the flow time.
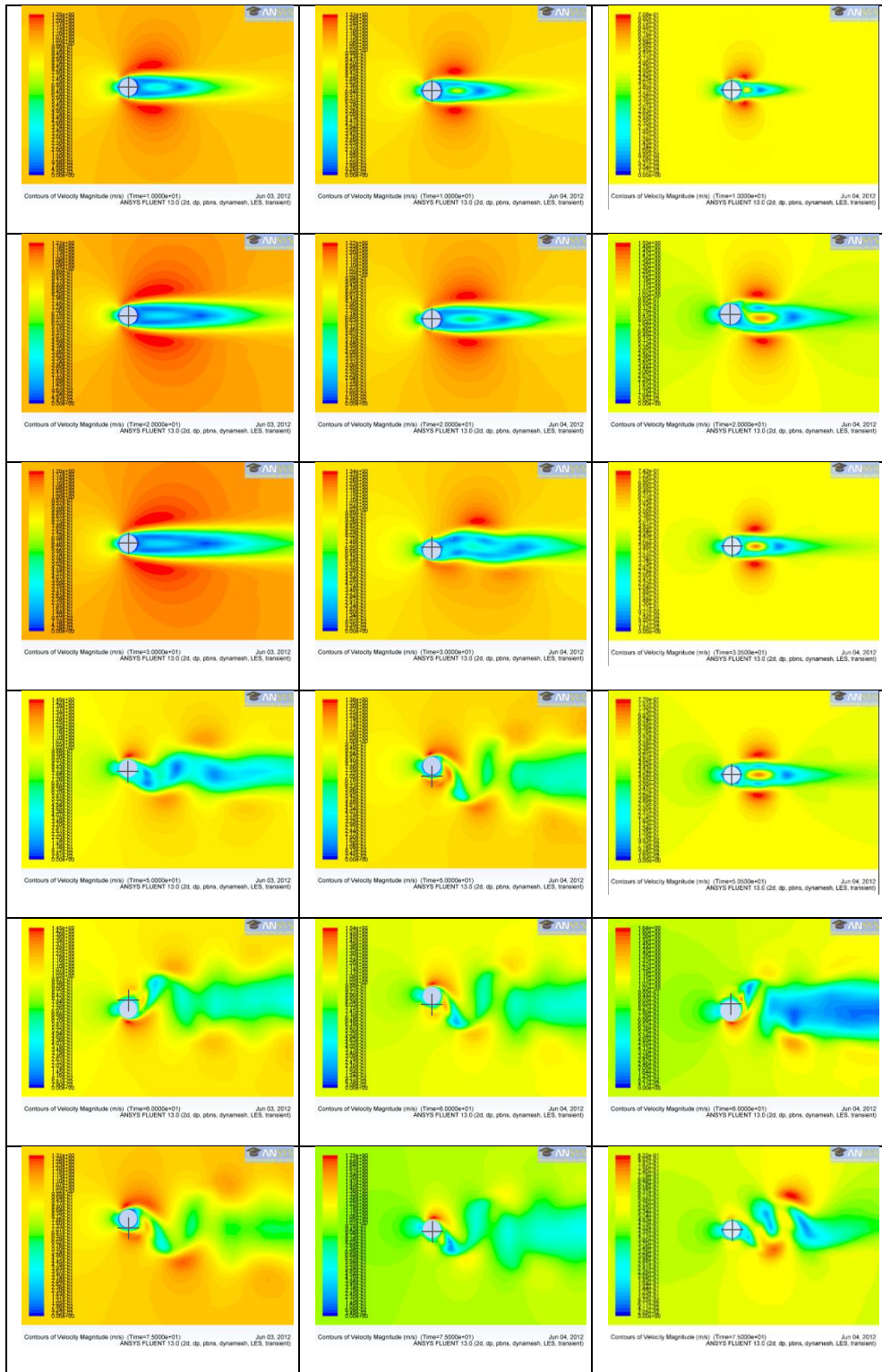
Figure 5.7. The development of the displacement as a function of flow time

6 CONCLUSIONS

The main part of this thesis focused on the characteristics of the flow pattern and vibration of the cylindrical structure due to the incompressible laminar and turbulent flow. The software package, FLUENT, has been used to perform the flow simulations for Re 40, 100, 200 and 1000.

This chapter is divided into two sections. The first section describes the most important conclusions that are obtained from the performed simulation. The second section presents some recommendation for further work within this subject.

6.1. Conclusion

The next lines present the conclusion of the thesis work as follow:

1. The flow characteristics of the steady laminar case at Re = 40, which is represented by the Cd value, length of recirculation zone, vortex centre location and the separation angle, shows a good agreement with the other studies.

2. The drag coefficient (Cd) at Re 100 shows a good agreement to the other studies. However, the lift coefficient (Cl) has a slight discrepancy compared to the other studies.

3. The implementation of the transient (unsteady) laminar flow for Re 200 and 1000 are perceived not accurate enough. The result shows that the Cd and Cl value has a poor agreement to the other studies. The use of the Large Eddy Simulation (LES) model improves the result significantly.

4. The largest cylinder displacement occurs when the lift force oscillates in sympathy with the cylinder motion. It means that the the vortex-shedding frequency, the vibration frequency and the natural frequency coincide ($f_v = f_{vib} = f_n$). In this simulation, the maximum displacement occurs at $U_{red,true} = 5.13$ (Re = 200).

6.2. Recommendations

1. The success of the CFD simulation depends on many factors, for instance the domain shape, mesh/grid shape and size, solver and etc. The choices of these factors influence the simulation time and result. For that reasons, specific studies to optimize setup are recommended.

2. The simulation set up in this thesis can be used for further analysis of vibration due to the flow effect. For instance, to assess the galloping, drag crisis or flow interaction in group of cylinders.

3. Even though flow around cylindrical structures is a classical subject and many studies have been carried out, it is still an interesting and relevant field to investigate and study.

REFERENCES

[1]   ANSYS. 2010. **ANSYS Meshing User's Guide.** ANSYS, Inc. Canonsburg, USA.

[2]   ANSYS. 2010. **ANSYS Fluent Theory Guide.** ANSYS, Inc. Canonsburg, USA.

[3]   Berthelsen, P.A. and Faltinsen, O.M. 2007. **A local directional ghost cell approach for incompressible viscous flow problems with irregular boundaries**. Journal of Computational Physic 227 (2008) 4354 – 4397.

[4]   Calhoun, D. 2002. **A Cartesian grid method for solving the two-dimensional streamfunction-vorticity equations in irregular regions**. Journal of Computational Physic. 176 (2) 231–275.

[5]   Drescher, H. 1956. **Messung der auf querangestriimte Zylinder ausgeubten zeitlich veriinderten Drucke**. 2. f. Flugwiss, 4(112):17-21.

[6]   Feng, C.C. 1968. **The measurements of the vortex induced effects in flow past stationary and oscillating circular and D-section cylinders**. Thesis, The University of British Columbia.

[7]   Ferziger, J.H and Peric, M. 1997. **Computational Methods for Fluid Dynamics**. Springer. Berlin-Germany.

[8]   Franke, R. et al. 1990. **Numerical Calculation of Laminar Vortex Shedding Flow Past Cylinders**. Journal of Wind Engineering and Industrial Aerodynamics, 35 (1990) 3237-257. Elsevier. Amsterdam.

[9]   Herfjord, K. 1996. **A study of two-dimensional separated flow by a combination of the finite element method and Navier–Stokes equations**. Dr. Ing.-Thesis, Norwegian Institute of Technology, Department of Marine Hydrodynamics. Trondheim, Norway.

[10] Launder, B.E. and Spalding, D.B. 1972. **Lectures in Mathematical Models of Turbulence**. Academic Press. London, England.

[11] Linnick, M. N and Fasel, H.F. 2005.**A high-order immersed interface method for simulating unsteady compressible flows on irregular domains**. J. Comput. Phys. 204 (1) 157–192.

[12] Rajani, B.N. et al. 2008. **Numerical Simulation of Laminar Flow Past a Circular Cylinder**. Journal of Applied Mathematical Modelling 33 (2009) 1228-1247. Elsevier.

[13] Russel, D. and Wang, Z.J. 2003. **A Cartesian grid method for modeling multiple moving objects in 2D incompressible viscous flow.** Journal of Computational Physic. 191 (1) 177–205.

[14] Sumer B.M. and Fredsøe J. 2006. **Hydrodynamics Around Cylindrical Structure**. World Scientific Publishing Co Pte. Ltd. Singapore.

[15] Versteeg H.K. and Malalasekera, W. 2007. **An Introduction to Computational Fluid Dynamics : The Finite Volume Method**. Pearson Prentice Hall. England

[16] Wilcox, D.C. 1998. **Turbulence Modelling for CFD**. DCW Industries, Inc. La Canada. California.

[17] Xu, S. and Wang, Z.J. 2006. **An immersed interface method for simulating the interaction of a fluid with moving boundaries**. Journal of Computational Physic. 216 (2) 454–493.

APPENDIXES – A
Problem Description

Consider a fluid flowing pass a cylinder, as illustrated below. The cylinder is considered as a fixed or a free oscillating body. The flow is expressed by the Reynolds number 40, 100, 200 and 1000.

Diameter of the pipe, $D = 1$ m
Flow velocity, $U = 1$ m/s
Density of the fluid, $\rho = 1$ kg/m^3.
Thus, the dynamic viscosity must be set,

$\mu = 0.025$ kg/m*s (Re = 40)
$\mu = 0.01$ kg/m*s (Re = 100)
$\mu = 0.005$ kg/m*s (Re = 200)
$\mu = 0.0001$ kg/m*s (Re = 1000)
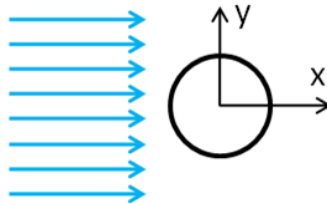
Figure 1. Simulation illustration.

The simulation will be carried out as indicated in following table.

Re	Steady	Unsteady	Laminar	Turbulent (LES)	Fixed Cylinder	Free Oscillating
40	x		x		x	
100	x	x	x	x	x	x
200	x	x	x	x	x	x
1000	x	x	x	x	x	x

Simulation objectives

Try to obtain :

1. Lift and Drag Coefficient (Cd and Cl)
2. The vortex shedding frequency (f_v)
3. Strouhal Number (St)
4. Vibration frequency (f_{vib})
5. The Amplitude of the vibration (A)

Solution Domain

A rectangular domain will be used for the simulation. The dimension of the domain is 60D x 90D.
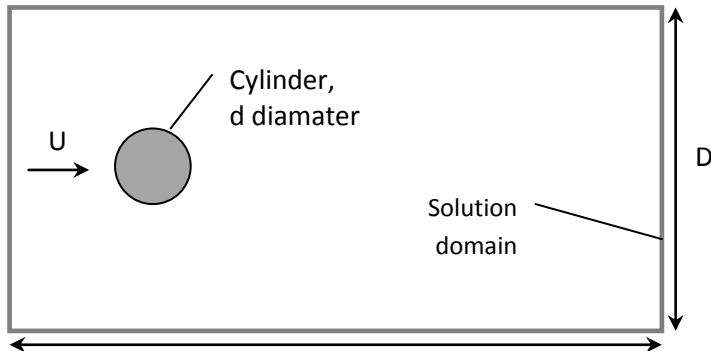
Figure 2. Solution domain sketch.

Boundary Conditions

First, we will specify a velocity inlet boundary condition. We will set the left side boundary as a velocity inlet with a velocity of 1 m/s in the x direction. Next, we will use a pressure outlet boundary condition for the right side boundary with a gauge pressure of 0 Pa. Lastly, we will apply a no slip boundary condition to the cylinder wall. The aforementioned boundary conditions are illustrated below.
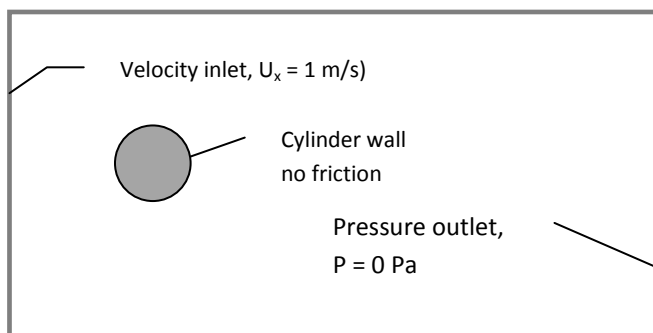
Figure 3. Boundary condition sketch.

APPENDIXES – B
User Define Function

This is the user define function (UDF) used in Fluent to define the motion of the cylinder due to the flow. It is the six degree of freedom (6DOF) solver, which is used when the movement of the rigid body is determined by the forces of the flow.

```c
#include "udf.h"

DEFINE_SDOF_PROPERTIES(sdof_props, prop, dt, time, dtime)
{
        real cg;
        real k = 1*1.26*1.26;
        cg = DT_CG(dt)[1];
        prop[SDOF_MASS] = 1;
        prop[SDOF_LOAD_F_Y] = -k*cg;
        prop[SDOF_ZERO_TRANS_X] = TRUE;
        prop[SDOF_ZERO_ROT_X] = TRUE;
        prop[SDOF_ZERO_ROT_Y] = TRUE;
}
```

APPENDIXES – C
Fluent Simulation Setup

This is the summary of the Input Setup of the simulation of the Steady Laminar Case, Re = 40.

FLUENT
Version: 2d, dp, pbns, lam (2d, double precision, pressure-based, laminar)
Release: 13.0.0
Title:

Models

```
  Model              Settings
  ------------------------------------
  Space              2D
  Time               Steady
  Viscous            Laminar
  Heat Transfer          Disabled
  Solidification and Melting   Disabled
  Species            Disabled
  Coupled Dispersed Phase     Disabled
  NOx Pollutants         Disabled
  SOx Pollutants         Disabled
  Soot           Disabled
  Mercury Pollutants       Disabled
```

Material Properties

  Material: aluminum (solid)

```
    Property          Units   Method    Value(s)
    --------------------------------------------------
    Density          kg/m3   constant  2719
    Cp (Specific Heat)   j/kg-k  constant  871
    Thermal Conductivity  w/m-k   constant  202.4
```

  Material: air (fluid)

```
    Property             Units    Method    Value(s)
    -------------------------------------------------------------
    Density              kg/m3    constant  1
    Cp (Specific Heat)       j/kg-k   constant  1006.43
    Thermal Conductivity      w/m-k    constant  0.0242
    Viscosity            kg/m-s   constant  0.025
    Molecular Weight        kg/kgmol  constant  28.966
    Thermal Expansion Coefficient  1/k     constant  0
    Speed of Sound          m/s      none      #f
```

Cell Zone Conditions

  Zones

    name   id   type
    ----
    surface_body 2   fluid

  Setup Conditions

    surface_body

      Condition   Value

      Material Name   air
      Specify source terms?   no
      Source Terms   ()
      Specify fixed values?   no
      Fixed Values   ()
      Frame Motion?   no
      Relative To Cell Zone   -1
      Reference Frame Rotation Speed (rad/s)   0
      Reference Frame X-Velocity Of Zone (m/s)   0
      Reference Frame Y-Velocity Of Zone (m/s)   0
      Reference Frame X-Origin of Rotation-Axis (m)   0
      Reference Frame Y-Origin of Rotation-Axis (m)   0
      Reference Frame User Defined Zone Motion Function   none
      Mesh Motion?   no
      Relative To Cell Zone   -1
      Moving Mesh Rotation Speed (rad/s)   0
      Moving Mesh X-Velocity Of Zone (m/s)   0
      Moving Mesh Y-Velocity Of Zone (m/s)   0
      Moving Mesh X-Origin of Rotation-Axis (m)   0
      Moving Mesh Y-Origin of Rotation-Axis (m)   0
      Moving Mesh User Defined Zone Motion Function   none
      Deactivated Thread   no
      Embedded Subgrid-Scale Model   0
      Momentum Spatial Discretization   0
      Cwale   0.325
      Cs   0.1
      Porous zone?   no
      X-Component of Direction-1 Vector   1
      Y-Component of Direction-1 Vector   0
      Relative Velocity Resistance Formulation?   yes
      Direction-1 Viscous Resistance (1/m2)   0
      Direction-2 Viscous Resistance (1/m2)   0
      Choose alternative formulation for inertial resistance?   no
      Direction-1 Inertial Resistance (1/m)   0
      Direction-2 Inertial Resistance (1/m)   0
      C0 Coefficient for Power-Law   0
      C1 Coefficient for Power-Law   0
      Porosity   1

Boundary Conditions

  Zones

    name   id   type
    ----
    inlet   10012   velocity-inlet
    cylinderwall   10013   wall
    outlet   10014   pressure-outlet
    wall-surface_body 5   wall

  Setup Conditions

    inlet

        Condition   Value

        Velocity Specification Method   1
        Reference Frame   0
        Velocity Magnitude (m/s)   0
        Supersonic/Initial Gauge Pressure (pascal) 0
        X-Velocity (m/s)   1
        Y-Velocity (m/s)   0
        X-Component of Flow Direction   1
        Y-Component of Flow Direction   0
        X-Component of Axis Direction   1
        Y-Component of Axis Direction   0
        Z-Component of Axis Direction   0
        X-Coordinate of Axis Origin (m)   0
        Y-Coordinate of Axis Origin (m)   0
        Z-Coordinate of Axis Origin (m)   0
        Angular velocity (rad/s)   0
        is zone used in mixing-plane model?   no

    cylinderwall

        Condition   Value

        Wall Motion   0
        Shear Boundary Condition   0
        Define wall motion relative to adjacent cell zone? yes
        Apply a rotational velocity to this wall?   no
        Velocity Magnitude (m/s)   0
        X-Component of Wall Translation   1
        Y-Component of Wall Translation   0
        Define wall velocity components?   no
        X-Component of Wall Translation (m/s)   0
        Y-Component of Wall Translation (m/s)   0
        Rotation Speed (rad/s)   0
        X-Position of Rotation-Axis Origin (m)   0
        Y-Position of Rotation-Axis Origin (m)   0
        X-component of shear stress (pascal)   0
        Y-component of shear stress (pascal)   0

Specularity Coefficient   0

outlet

   Condition   Value

   Gauge Pressure (pascal)   0
   Backflow Direction Specification Method   1
   X-Component of Flow Direction   1
   Y-Component of Flow Direction   0
   X-Component of Axis Direction   1
   Y-Component of Axis Direction   0
   Z-Component of Axis Direction   0
   X-Coordinate of Axis Origin (m)   0
   Y-Coordinate of Axis Origin (m)   0
   Z-Coordinate of Axis Origin (m)   0
   is zone used in mixing-plane model?   no
   Specify Average Pressure Specification   no
   Specify targeted mass flow rate   no
   Targeted mass flow (kg/s)   1
   Upper Limit of Absolute Pressure Value (pascal)   5000000
   Lower Limit of Absolute Pressure Value (pascal)   1

wall-surface_body

   Condition   Value

   Wall Motion   0
   Shear Boundary Condition   0
   Define wall motion relative to adjacent cell zone?   yes
   Apply a rotational velocity to this wall?   no
   Velocity Magnitude (m/s)   0
   X-Component of Wall Translation   1
   Y-Component of Wall Translation   0
   Define wall velocity components?   no
   X-Component of Wall Translation (m/s)   0
   Y-Component of Wall Translation (m/s)   0
   Rotation Speed (rad/s)   0
   X-Position of Rotation-Axis Origin (m)   0
   Y-Position of Rotation-Axis Origin (m)   0
   X-component of shear stress (pascal)   0
   Y-component of shear stress (pascal)   0
   Specularity Coefficient   0

Solver Settings

 Equations

   Equation   Solved

   Flow   yes

 Numerics

Numeric   Enabled

Absolute Velocity Formulation   yes

Relaxation

Variable   Relaxation Factor

Pressure   0.3
Density   1
Body Forces 1
Momentum   0.7

Linear Solver

         Solver   Termination Residual Reduction
Variable   Type   Criterion   Tolerance

Pressure   V-Cycle 0.1
X-Momentum Flexible 0.1   0.7
Y-Momentum Flexible 0.1   0.7

Pressure-Velocity Coupling

Parameter   Value

Type   SIMPLE

Discretization Scheme

Variable   Scheme

Pressure   Standard
Momentum   QUICK

Solution Limits

Quantity   Limit

Minimum Absolute Pressure   1
Maximum Absolute Pressure   5e+10
Minimum Temperature   1
Maximum Temperature   5000